9950-699

E83-10157

CR-169768

MDA

MACDONALD DETTWILER & ASSOCIATES LTD.

VANCOUVER, CANADA

SEASAT SAR PERFORMANCE EVALUATION STUDY
FINAL REPORT

00-0676-D00

Prepared for:

California Institute of Technology
Jet Propulsion Laboratory
4800 Oak Grove Drive
Pasadena, California 91103

Contract Number 956104

This work was performed for the Jet Propulsion Laboratory, California Institute of Technology, and sponsored by the National Aeronautics and Space Administration, under Contract NAS7-100.

Prepared by:

MacDonald, Dettwiler and Associates Ltd.
3751 Shell Road, Richmond, B.C., Canada, V6X 2W2
Telephone No.: (604) 278-3411

JUNE, 1982

MDA

MACDONALD DETTWILER & ASSOCIATES LTD.

VANCOUVER, CANADA

RESTRICTION ON DISCLOSURE OF DATA

SEASAT SAR PERFORMANCE EVALUATION STUDY
FINAL REPORT

00-0676-D00

Prepared for:

California Institute of Technology
Jet Propulsion Laboratory
4800 Oak Grove Drive
Pasadena, California 91103

JUNE, 1982

PREFACE

This report has been prepared in accordance with the requirements of JPL Contract Number 956104, titled "Seasat SAR Performance Evaluation Study", which is a subcontract under NASA contract NAS7-100. The report discusses the methodology and results of two investigations: amplitude calibration and location accuracy of Seasat SAR image data.

ABSTRACT

This report contains an evaluation of certain aspects of the performance of the Seasat SAR (Synthetic Aperture RADAR) sensor, using data processed by the MDA digital processor. Two particular aspects are studied: the location, accuracy of image data, and the calibration of the measured backscatter amplitude of a set of corner reflectors.

The assessment of the image location accuracy is done by selecting identifiable targets in several scenes, converting their image location to UTM coordinates, and comparing the results to map sheets. The error standard deviation is measured to be approximately 30 metres.

The amplitude calibration is performed by measuring the responses of the Goldstone corner reflector array and comparing the results to theoretical values. A linear regression of the measured against theoretical values results in a slope of 0.954 with a correlation coefficient of 0.970.

TABLE OF CONTENTS

TABLE OF ILLUSTRATIONS

* Actual Page Number

TABLE OF ILLUSTRATIONS

* Actual Page Number

MDA

1. INTRODUCTION

The purpose of this study was to evaluate certain aspects of the performance of the Seasat SAR. Specifically two investigations were undertaken with data processed by the MDA Seasat SAR processor. The first investigation was an evaluation of the location accuracy of Seasat SAR imagery, which is discussed in Section 2. The second investigation consisted of a calibration of the measured backscatter amplitude of a set of corner reflectors, and this is discussed in Section 3.

2. IMAGE LOCATION ACCURACY STUDY

2.1 Introduction

The purpose of the image location accuracy study is to determine the geometric accuracy in SAR imagery produced by the MDA Seasat processor. This is done by selecting several scenes of different terrain variations and in each scene selecting identifiable targets. Each target is mapped to UTM coordinates which are then compared to the coordinates read from a map sheet.

Section 2.2 briefly outlines the transformation from line, pixel coordinates in the image to UTM coordinates. Section 2.3 presents the experimental results and an analysis of the residual errors obtained in the experiment.

2.2 Transformation From Image Pixel Coordinates to UTM Map Coordinates

2.2.1 Slant Range/Azimuth to Map Projection Transformation

The process of transforming from slant range/azimuth (fast time/slow time) to the output map projection coordinates is grasped by a series of discrete transformations, beginning with the line/pixel coordinate in the input slant range image, as follows:

Line/Pixel	Image memory coordinates
↓	
τ_m, t_r	Fast time/slow time coordinates
↓	
x_s, y_s, z_s	Satellite coordinates
↓	
x_e, y_e, z_e	Earth Centred Rotating (ECR) coordinates
↓	
x, y	Map projection coordinates

These discrete transformations are specified in order below.

2.2.2 Image Memory to Satellite Coordinate System

Given a line and pixel coordinate in image, its fast time (τ_m) and slow time (t_k) can be computed from the auxiliary data. If this target has a Doppler frequency ν, the target's coordinates (x_s, y_s, z_s) in the satellite coordinate system can be solved from the intersection of three surfaces:

Doppler surface

$$m_x x_s + m_y y_s + m_z z_s = f(\nu) \qquad (1)$$

Wave front surface (free space; c = constant)

$$x_s^2 + y_s^2 + z_s^2 = (c\ \tau_m/2)^2 \qquad (2)$$

Earth surface

$$x_s^2 + y_s^2 + (z_s - H)^2 = r^2 \qquad (3)$$

where

$f(\nu)$	=	a function of Doppler frequency
H	=	satellite distance from earth centre
r	=	planet radius at target location
c	=	velocity of propagation in free space
m_x, m_y, m_z	=	functions of spacecraft velocity and position

In this coordinate system, the z_s axis points to the centre of the earth and the coefficients m_x, m_y, and m_z of the Doppler surface are

chosen such that the y_s axis points in the real track direction. By solving the equations representing the three surfaces, it can be shown that:

$$\begin{bmatrix} x_s \\ y_s \\ x_s \end{bmatrix} = \begin{bmatrix} \pm\sqrt{\frac{C\tau_m^2}{2} - y_s^2 - z_s^2} \\ [f(v) - m_x x_s - m_z z_s] / m_y \\ \left(\left(\frac{C\tau_m}{2}\right)^2 + H^2 - r^2 \right) / 2H \end{bmatrix} \qquad (4)$$

The MDA Seasat processor compresses a target to its zero Doppler position and hence, $v = 0$.

The value of x_s is positive for a radar clock angle of 270° and negative for a clock angle of 90°. The value of r is target position dependent and requires the use of a planetary datum, plus the planetary coordinates of the target, and incorporates a DTM elevation above the datum.

2.2.3 Satellite Coordinates to Earth Centred Rotation Coordinates System

The relation between the satellite coordinate system and ECR coordinate system is shown in Figure 2.2-1. The coordinates of the target in the ECR coordinate system are given by:

$$\begin{bmatrix} x_e \\ y_e \\ z_e \end{bmatrix} = M(t_k) \begin{bmatrix} x_s \\ y_s \\ z_s \end{bmatrix} + \begin{bmatrix} \Delta x \\ \Delta y \\ \Delta z \end{bmatrix} \qquad (5)$$

where $M(t_k)$ is the rotation matrix (dependent on spacecraft velocity and position) for mapping a vector from the satellite coordinates to the ECR coordinates and $(\Delta x, \Delta y, \Delta z)^T$ is the displacement vector between the two coordinate systems. The vector $(x_s, y_s, z_s)^T$ is a function of τ_m and has been defined in Equation 4. These target coordinates are used to compute the earth radius r from the earth centre for refinement of Equation 4 due to planet asphericity. The system of Equations 4 and 5 must be solved self-consistently to result in a precise value for the target earth coordinates.

ORIGINAL PAGE IS
OF POOR QUALITY

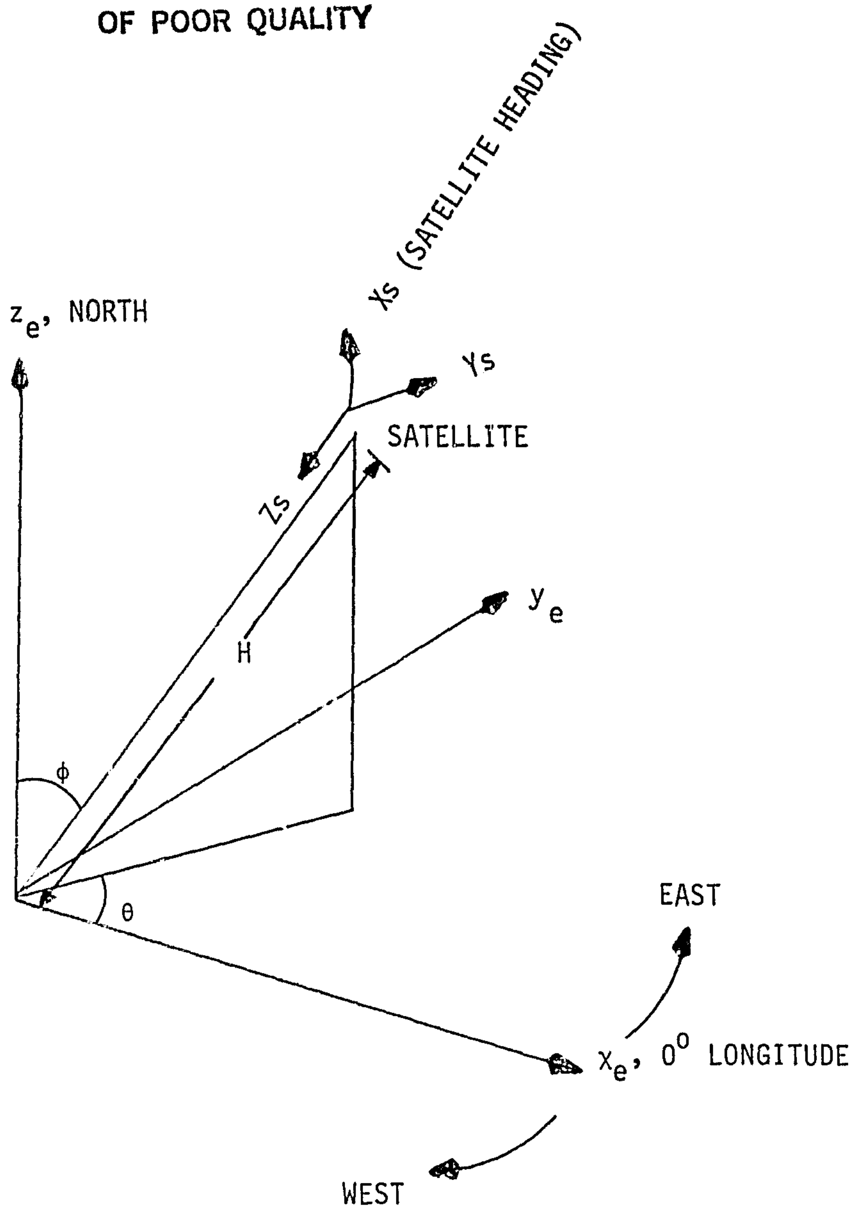

FIGURE 2.2-1 SATELLITE AND EARTH CENTRED ROTATING COORDINATES

2.2.4 ECR to Map Projection Transformation

The map projection coordinates (x, y) are functions of (x_e, y_e, z_e):

$$x = g_1 (x_e, y_e, z_e)$$

$$y = g_2 (x_e, y_e, z_e)$$

The functions g_1 and g_2 depend on the map projection specified. The transformation from ECR coordinates to UTM coordinates or any other map projection coordinates can be found in any standard map projection text [1].

2.3 Experiment and Determination of Point Location Errors

The experiment consisted of the following procedures:

1. Produce five Seasat SAR images on the MDA Seasat processor.

2. Select at least 16 clearly distinguishable and locatable targets in each of the images.

3. From topographic maps, determine the location and elevation of these targets.

4. Using only the location of the target within an image, as well as Goddard Space Flight Centre supplied Definitive Orbit Record data, predict the location of each of these targets, correcting for each target's elevation.

5. Determine the means and standard deviation of the differences in locations derived from Steps 3 and 4.

The scenes used for the experiments were selected with the following criteria:

- each scene has an adequate number of identifiable targets;

- the scenes cover a substantial range of the available orbits; and

- at least two receiving stations be involved.

The scenes selected were as follows:

- Ottawa, Ontario - Orbit 472
- Pembroke, Ontario - Orbit 1218

- Niagara Falls, Ontario - Orbit 1218
- Vancouver, B.C. - Orbit 230
- Vancouver Island, B.C. - Orbit 474

The first three scenes were received at Shoe Cove, Newfoundland, while the last two were received at Goldstone, California. In all five scenes, the satellite was in a descending node. Although it would have been desirable, no suitable ascending node scenes were available.

The maps used were 1:50,0000 class A1 and class C3 maps. Each map is on a UTM grid. A class A1 map has the following accuracy:

- horizontal 90% within 25 m (σ = 15 m)
- vertical 90% within 25 m (σ = 15 m)
- elevation 90% within ½ contour interval (σ = 0.30 contour interval)

For class C3 maps, the σ values in the three directions are three times as large as the corresponding values for A1 maps.

Figures 2.3-1 to 2.3-5 show the five scenes and the targets on each scene are marked. These five scenes vary from relatively flat terrain (e.g., Pembroke) to very rugged terrain (e.g., Vancouver Island and the north shore of Vancouver). Experimental results are summarized in Table 2.3-1, which gives the along and across track errors. The class of maps used and contour intervals are shown in Table 2.3-2.

The positive sense of the along and across track errors for a target is as shown in Figure 2.3-6.

TABLE 2.3-1 ALONG TRACK AND ACROSS TRACK ERRORS

Scene	Number of targets	Along Track bias in metres	Across Track bias in metres	Along Track* σ/RMS in metres	Across Track* σ/RMS in metres
Ottawa	17	- 47	35	33/57	38/52
Pembroke	19	-6186	54	24/6186	38/66
Niagara Falls	16	-6154	407	33/6154	31/408
Vancouver	21	- 151	24	40/156	64/68
Vancouver Island	18	- 399	35	29/410	78/85

*Note: σ is the standard deviation

TABLE 2.3-2 MAPS AND CONTOUR INTERVALS FOR THE SCENES

Scene	Number of targets	No. of targets in class A1 map			No. of targets in class C3 map		
		25 ft. C.I.	50 ft. C.I.	100 ft. C.I.	25 ft. C.I.	50 ft. C.I.	100 ft. C.I.
Ottawa	17	12	5				
Pembroke	19	8	11				
Niagara Falls	16	16					
Vancouver	21	5	12				4
Vancouver Island	18		3				15

C.I. = contour interval

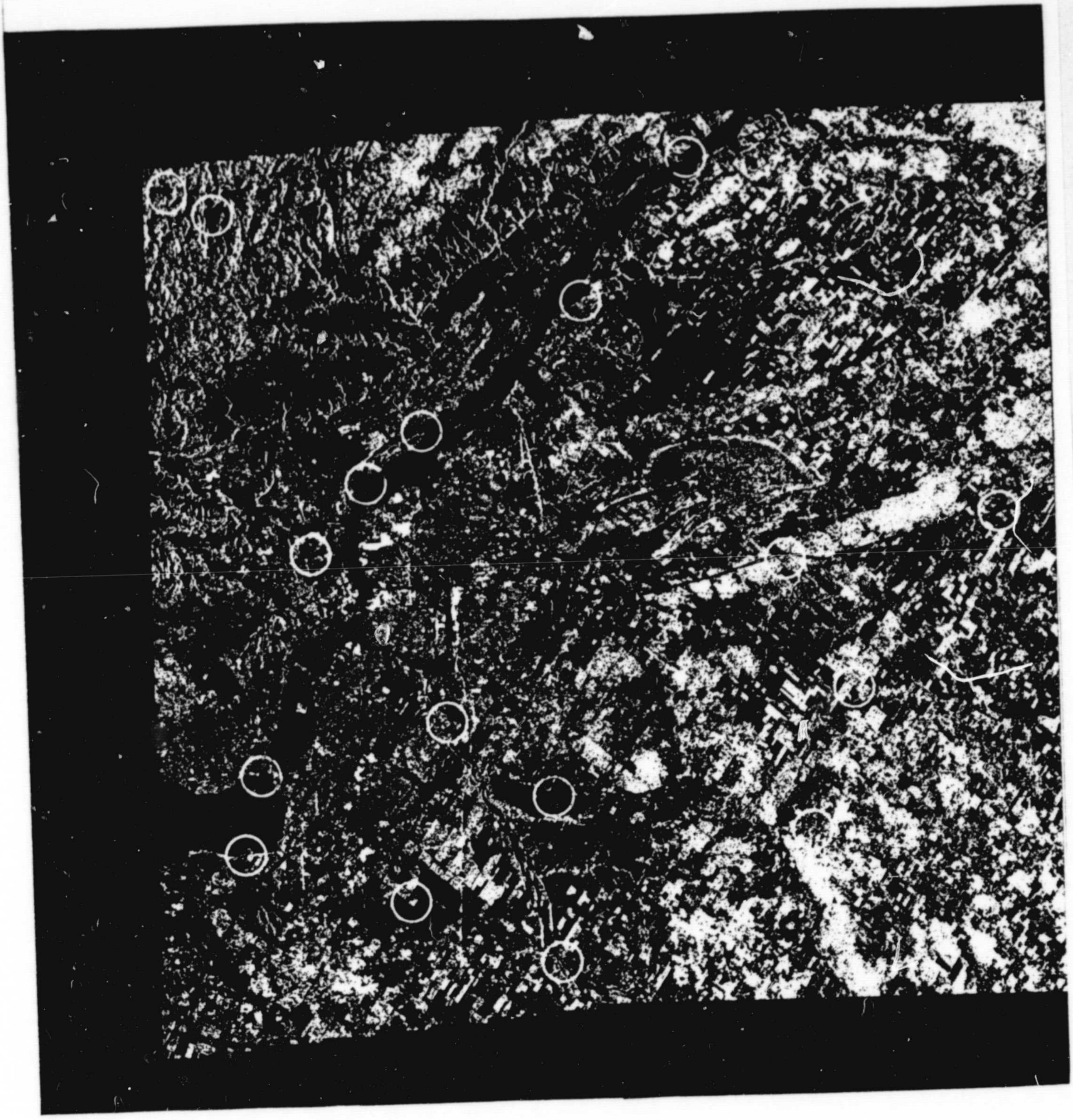

FIGURE 2.3-1 OTTAWA SCENE

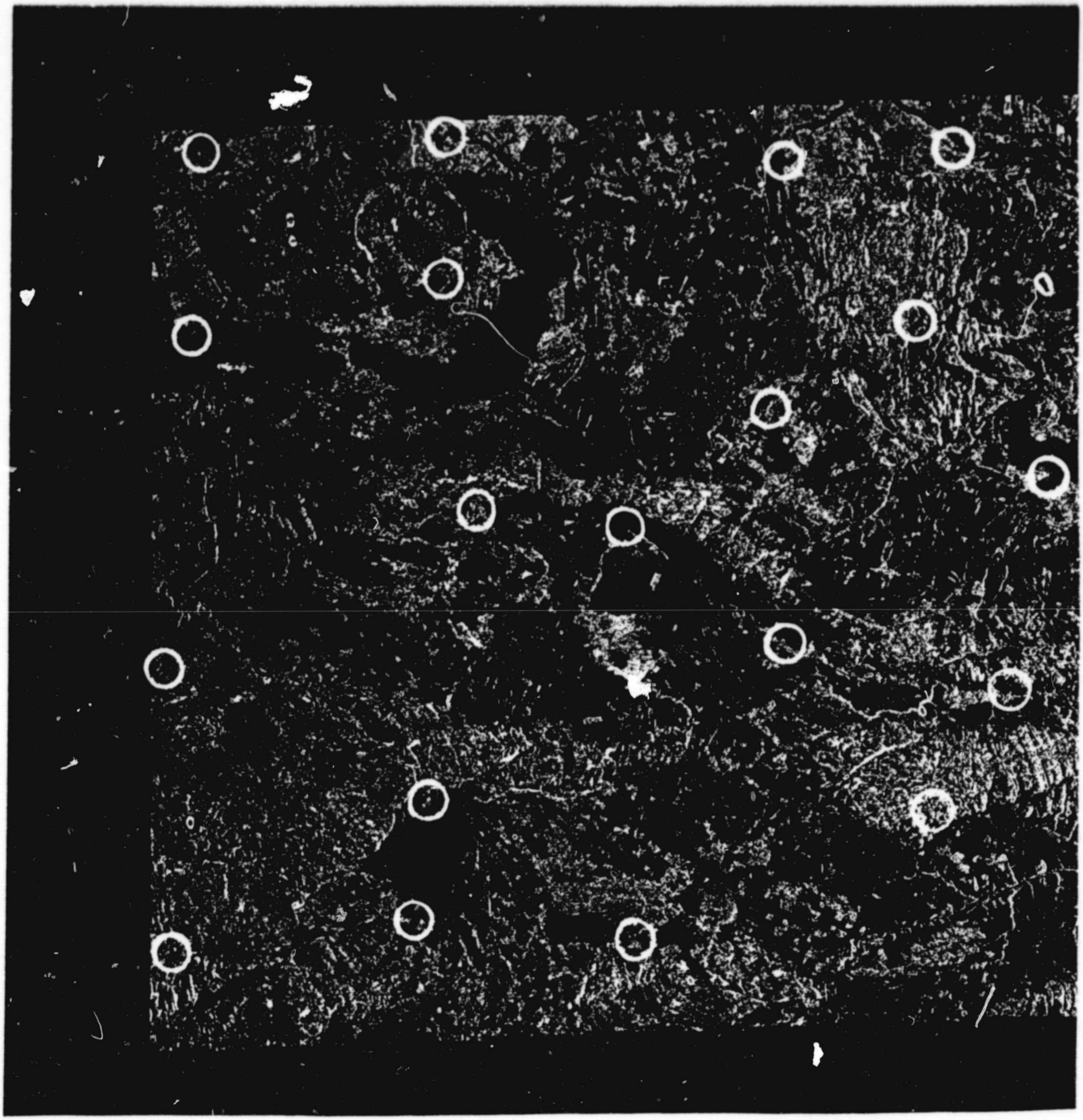

FIGURE 2.3-2 PEMBROKE SCENE

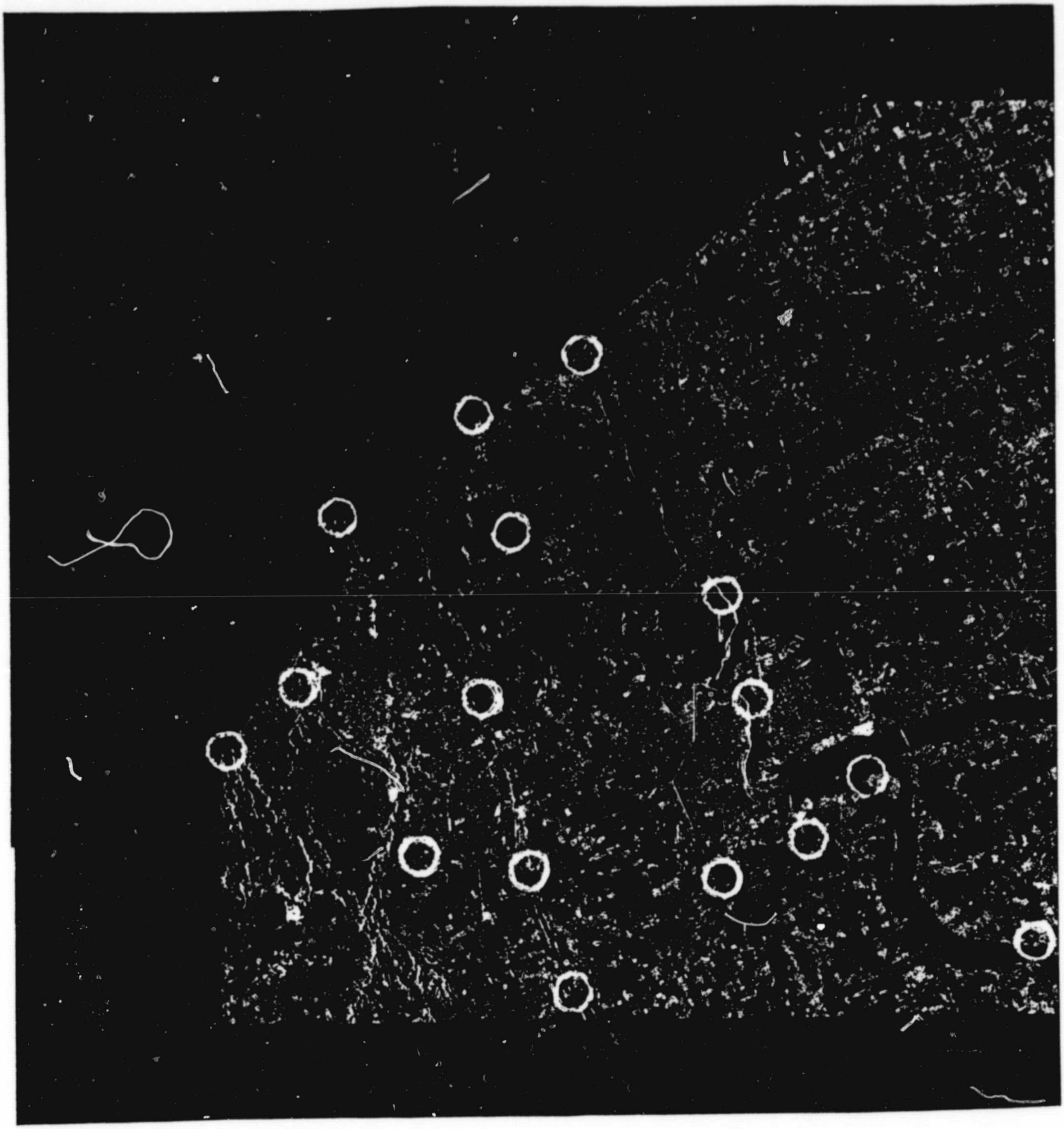

NOTE:

No GCPs were marked in the U.S. side because maps of about 1:25000 scale were not available at the time of the experiment.

FIGURE 2.3-3 NIAGARA FALLS SCENE

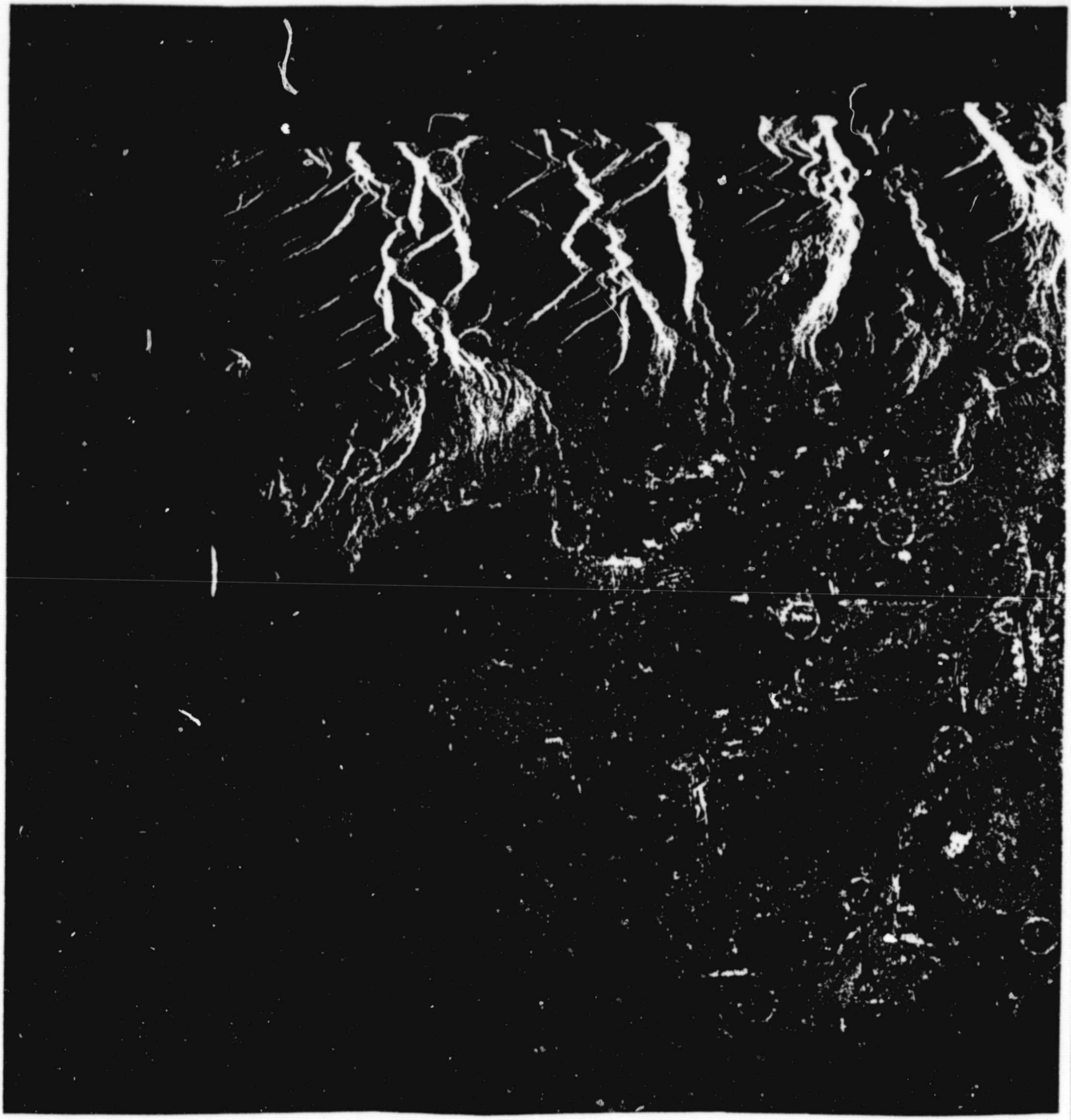

FIGURE 2.3-4 VANCOUVER SCENE

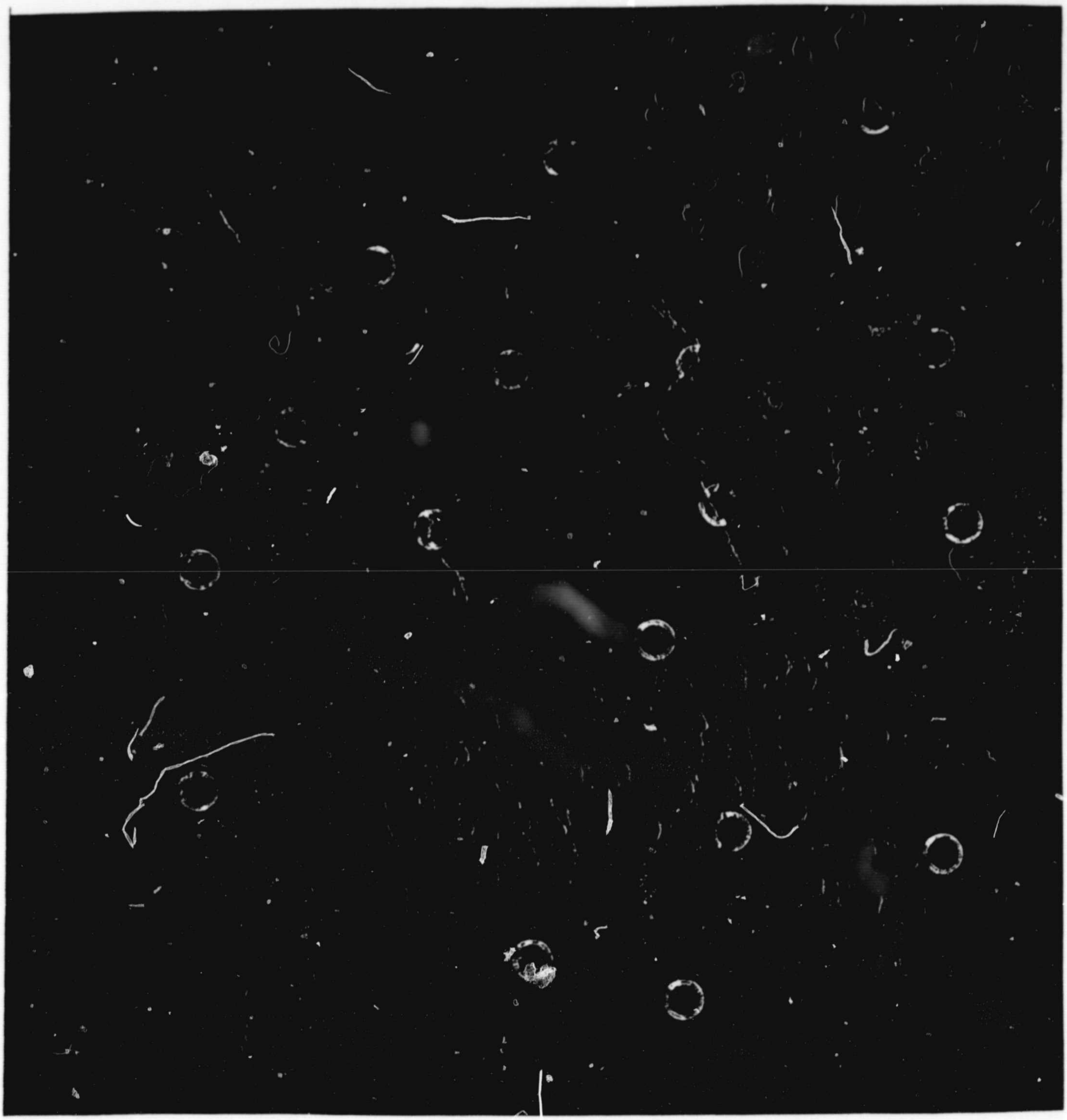

FIGURE 2.3-5 VANCOUVER ISLAND SCENE

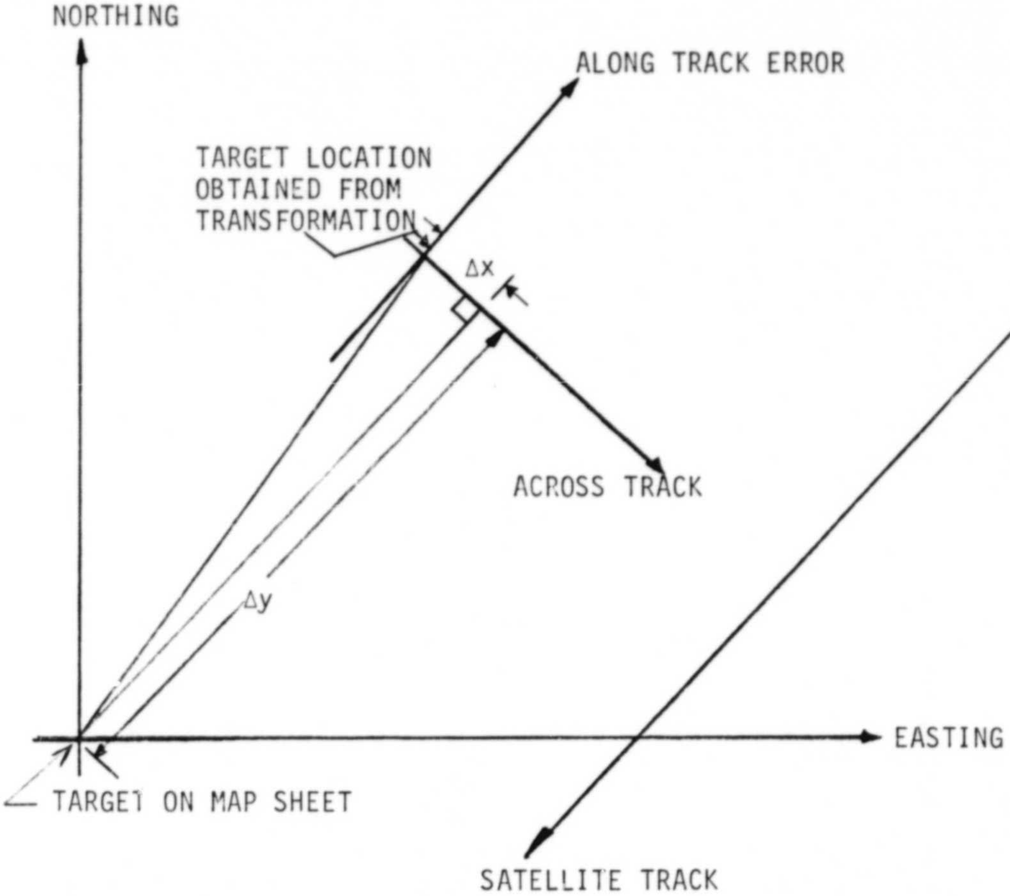

In this example,

Along track error = Δy
Across track error = Δx

FIGURE 2.3-6 ALONG TRACK AND ACROSS TRACK ERRORS

Table 2.3-1 shows two types of errors:

- Absolute or mean error with bias in the along and across track direction,

- Relative error after bias removal and expressed in terms of standard deviation.

The across track bias in four out of five scenes lies below 54 metres. Only in one scene (Niagara Falls), the bias reaches 407 metres which is approximately equivalent to a 0.9 microsecond error in range (fast time). Another source of the along track bias is due to processing error as a result of inaccuracy in the azimuth match filter FM rate. It can be shown that typically, this introduces an along track bias of 40 metres over the entire scene.

The along track error varies quite drastically from scene to scene. In three scenes, it is less than 400 metres, while in the two other scenes, it exceeds 6000 metres. These two scenes (Pembroke and Niagara Falls) are in the same orbit and the huge bias is believed to result from a time error in the receiving station clock of approximately one second.

The relative error is caused by:

- Marking a target line, pixel location in image from which a pixel corresponds to 12.5 metres on the ground. In the experiment, each target was marked on a standard video monitor display and in this process, a maximum error of 1½ pixel was estimated in the along track and across track directions. Assuming uniform error distribution, the standard deviation in each direction is then 0.866 pixel, or 11 metres.

- Marking of target location on a map sheet. In a 50,000 scale map sheet, a placement error of 1 mm corresponds to 50 metres was estimated in the along track and across track directions. Assuming uniform error distribution, the standard deviation in each direction is then 14 metres.

- Map accuracy. For class A1 1:50,000 map sheets, the spatial RMS error is 15 metres in easting and northing directions (also 15 metres in along track and across track). For class C3 maps, these RMS values are 46 metres.

- Orbit ephemeris data error. The Definitive Orbit Record data supplied by the Goddard Space Flight Centre contains satellite position information once every minute. The error for each position is [4]:

  σ in along track = 17 metres
  σ in across track = 10 metres

  For each scene, five points with the scene within the two end points were used to define a quartic polynomial fit to the satellite position. This has been shown to give an error of less than 1.2 metres in each direction. Hence, the ephemeris interpolation error is negligible.

- Terrain displacement. This has effect only in the across track direction. As has been mentioned, σ for elevation error is 0.3 contour interval for class A1 maps. On gently rolling areas, the contour interval is 25 feet. On hilly areas, it can be 50 feet or 100 feet. Then for gently rolling areas, σ (class A1 map) = 2.29 metres. This corresponds to six metres on ground displacement, since for every metre in height relief displacement is 2.7 metres on the ground. For 100 foot contour intervals and class C3 maps σ for elevation error is 0.9 times the contour interval (i.e., 27.43 metres), and hence, σ for relief displacement is 74 metres on the ground.

- Contour Interval Interpolation error. This again which has effect only in the across track direction. Usually a target does not fall onto a contour line in the map sheet; the target height has to be interpolated. As interpolation accuracy of ¼ contour interval was estimated. Thus, for a contour interval of 25 feet and assuming uniform distribution in interpolation error, σ (class A1 map) = 1.1 metres. This corresponds to 3 metres in relief displacement. For 100 foot contour intervals, the corresponding value for class C3 map is 36 metres.

The expected overall σ was calculated for each scene and the result is shown in Table 2.3-3. In the calculation, the map sheet class and contour interval have been taken into account.

The experimental location errors agree fairly well with the predicted values for all five scenes as shown in Table 2.3-3. Note that the predicted and experimental across track errors increase with terrain elevation. This is verified by removing the highest targets in the mountains in the Vancouver and Vancouver Island scenes. The final result is shown in Table 2.3-4. Relief displacement is most significant in the Vancouver Island scene where most targets are marked in mountainous areas. In this scene, across track σ is 78 metres but along track σ is 29 metres.

Results in Table 2.3-4 still show that the experimental error is slightly higher than predicted in the first four scenes even though the targets in hilly areas are not considered. This is probably due to a combination of the following factors:

- Some map sheets may not be in class A1 as claimed. For class B2 maps, the corresponding expected σ's are 40 metres in the along track and across track.

- Measurement error on video monitor may have exceeded what was quoted earlier; i.e., measurement error.> 1½ pixels.

ORIGINAL PAGE IS
OF POOR QUALITY

TABLE 2.3-3 PREDICTED/EXPERIMENTAL ERROR

Scene	Along Track σ in metres Predicted	Along Track σ in metres Experimental	Across Track σ in metres Predicted	Across Track σ in metres Experimental	Terrain Description
Ottawa	30	33	27	38	some hills
Pembroke	29	24	26	38	gently rolling
Niagara Falls	29	33	26	31	gently rolling
Vancouver	35	40	48	64	some high mountains
Vancouver Island	49	29	87	78	very mountainous

TABLE 2.3-4 COMPARISON OF ALONG TRACK AND ACROSS TRACK ERRORS WITH AND WITHOUT TARGETS IN HILLY AREAS

Scene	Number of targets	Along track σ metres	Across track σ in metres
Vancouver	17	42/40	40/64
Vancouver Island	14	24/29	47/78

Note: a/b

a = value when targets in hilly areas not taken into account.

b = value when those targets taken into account.

- Measurement error on map sheet may have exceeded what was quoted earlier; i.e., measurement error > ½ mm.

2.4 Conclusions

Five scenes of different terrain variations have been used in the experiment and at least 16 targets have been selected in each scene. Highlights of the experimental results are:

- The across track bias is small while the along track bias can be as large as 6 km. This along track error is most probably due to a timing error in the station clock of about one second.

- After bias removal, the error standard deviation in the along track direction is about 30 metres and in relatively flat areas, this value is about the same in across track direction.

- The errors (after bias removal) are due to marking of targets on the video monitor and on the map sheet, map accuracy, orbit ephemeris data error, and terrain interpolation error.

- After bias removal, the error standard deviation in the across track direction can be as much as 80 metres in hilly areas. This is aggravated by targets with high elevations. By not considering these targets, the standard deviation decreases considerably in each direction. The problems with hilly areas are coarser contour intervals (50 feet or 100 feet), larger terrain interpolation error and target identification problems due to radar layover.

The image location error founded in this experiment has two components: radar image registration error and target identification (both on the mapsheet and the COMTAL) error. When using the radar as a mapping tool, the resulting error consists only of the radar image registration error component; thus, the mapping error is less than the values obtained in the experiment.

3. AMPLITUDE CALIBRATION EXPERIMENT

3.1 Introduction

The ability to accurately measure the Radar Cross-Section (RCS) or backscatter amplitude of targets from SAR images is of major importance for a variety of uses such as crop identification and ice surveillance. In order to do this, the measured amplitude at the output of a SAR processor must be calibrated with known true values, in order to estimate and remove the effects of unknown gains that occur throughout the SAR system. As in any real system, non-linearities are also induced that should be taken into account [2] by the calibration procedure.

This section details the calibration that was performed with imagery of the Goldstone target array as processed by the MDA Seasat SAR digital processor (AP version). Section 3.2 gives a summary description of the target array. Descriptions of the analysis software and resulting measurement errors are given in Section 3.3. Section 3.4 gives the test results, while Section 3.5 gives a summary and conclusions.

3.2 Goldstone Target Array

The Goldstone array was a collection of ten corner reflectors situated on a dry lake bed near the Goldstone Satellite Receiving Station. Four classes of trihedral reflectors were used: 8 foot square, and 8, 6, and 4 foot triangular. The reflectors were arranged as shown in Figure 3.2-1. The triangular reflectors were erected with their boresights in the vertical direction to accommodate both ascending and descending orbit passes. The square reflectors, however, were tilted and oriented with their boresights aligned with the satellite during ascending passes. The target lettering is used for identification purposes in Section 3.4.

Table 3.2-1 and the accompanying figure gives the physical dimensions and RCSs of the reflectors [3]. The actual cross-section of a 6 foot triangular reflector was measured on a test range and found to be 0.23 dB below the theoretical value, which is believed to be within the measurement error. As the triangular reflectors were illuminated off the boresights, their RCSs were reduced by 4.6 dB. It should be noted that the two large square reflectors were of poorer construction, and hence their response could easily be 2 dB less than that calculated.

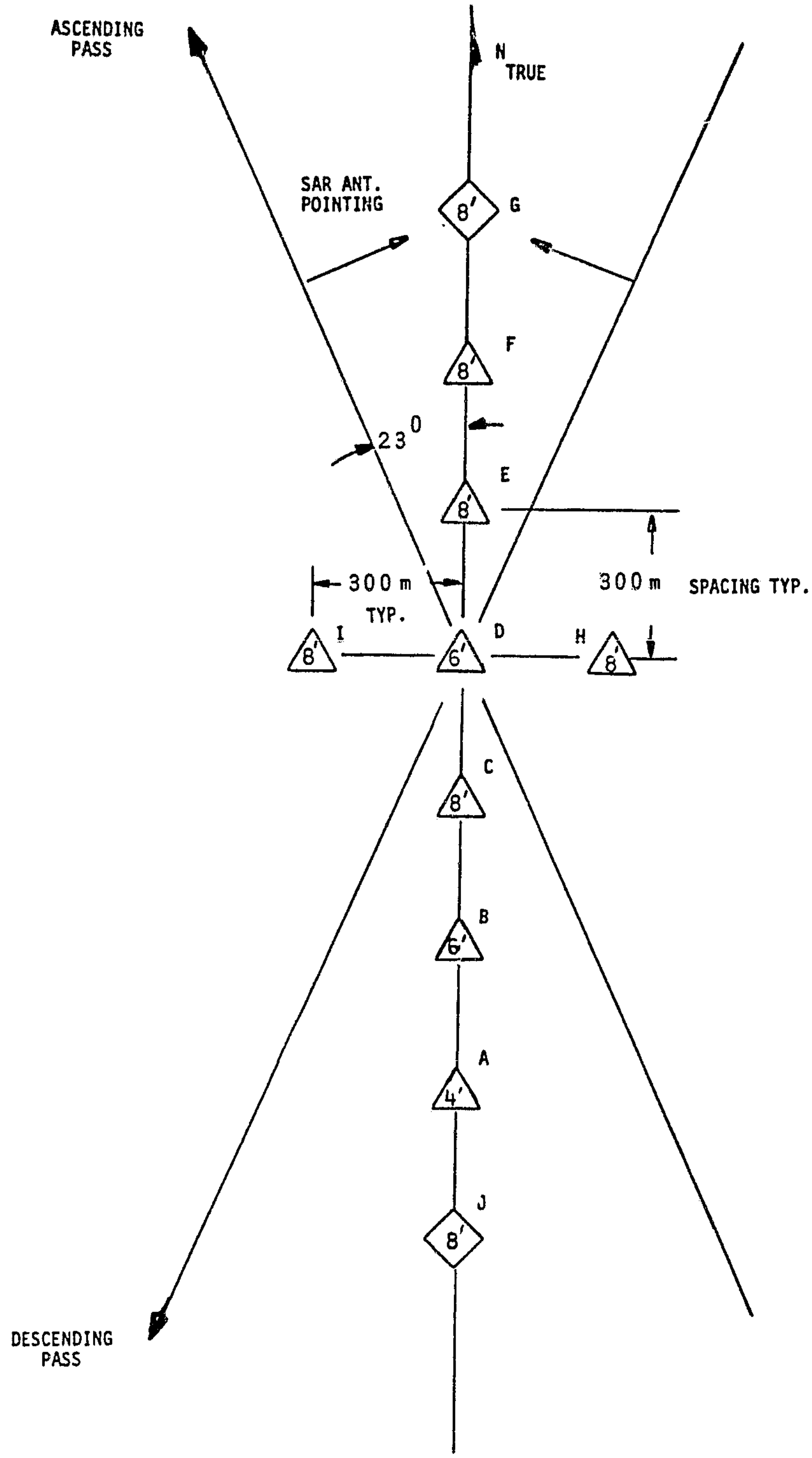

FIGURE 3.2-1 GOLDSTONE TARGET ARRY

ORIGINAL PAGE IS
OF POOR QUALITY

TABLE 3.2-1 REFLECTOR CROSS-SECTIONS

Trihedral Reflector

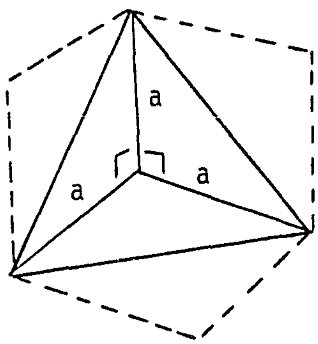

RCS:

Triangular Plates	Square Plates
$\frac{4\pi a^4}{3\lambda^2}$	$\frac{12\pi a^4}{\lambda^2}$

Size	"a" (actual) metres	RCS max (calculated) dBsm	RCS max (measured) dBsm	RCS @23^0 off boresight dBsm
8' (square)	2.438	43.81	--	--
8' (triangle)	2.432	34.23	--	29.63
6' "	1.790	28.91	28.69	24.09
4' "	1.188	21.77	--	17.17

3.3 Analysis Software

The analysis software used consisted mainly of a two-dimensional FFT interpolator followed by a measurement of the peak amplitude, peak location and 3 dB widths, as well as plots of their responses. To evaluate any measurement error that might be induced by the analysis software itself, a series of tests were carried out using simulated targets of varying resolutions with varying locations within a pixel.

The simulated targets were of the form:

$$f\,(x,\,y) = A\,\sqrt{\left(\frac{\sin\,(c_x\;\;(x - x_0))}{c_x\,\pi\,(x - x_0)}\right)^2 \left(\frac{\sin\,(c_y\,\pi\,(y - y_0))}{c_y\,\pi\,(y - y_0)}\right)^2}$$

where:

A	=	amplitude gain
c_x	=	line scaling factor
c_y	=	pixel scaling factor
x_0	=	line peak location
y_0	=	pixel peak location

The relation between scaling factor ($c_{x,\,y}$) and 3 dB width ($\rho_{x,\,y}$) is:

$$c_{x,y} = \frac{0.8859}{\rho_{x,y}}$$

ORIGINAL PAGE IS
OF POOR QUALITY

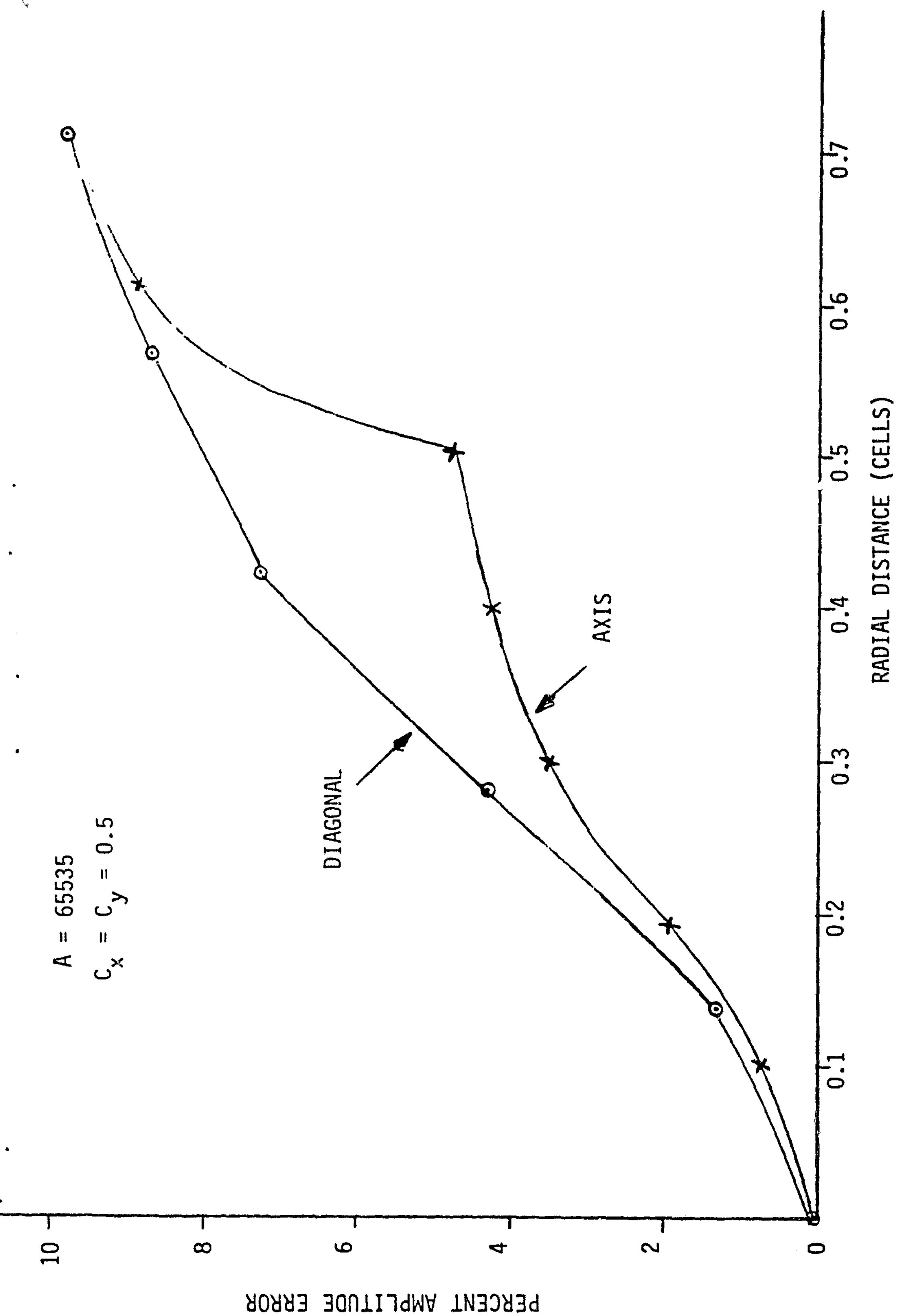

FIGURE 3.3-1 PERCENTAGE AMPLITUDE ERROR VS. PEAK RADIAL DISTANCE FROM LINE/PIXEL INTERSECTION

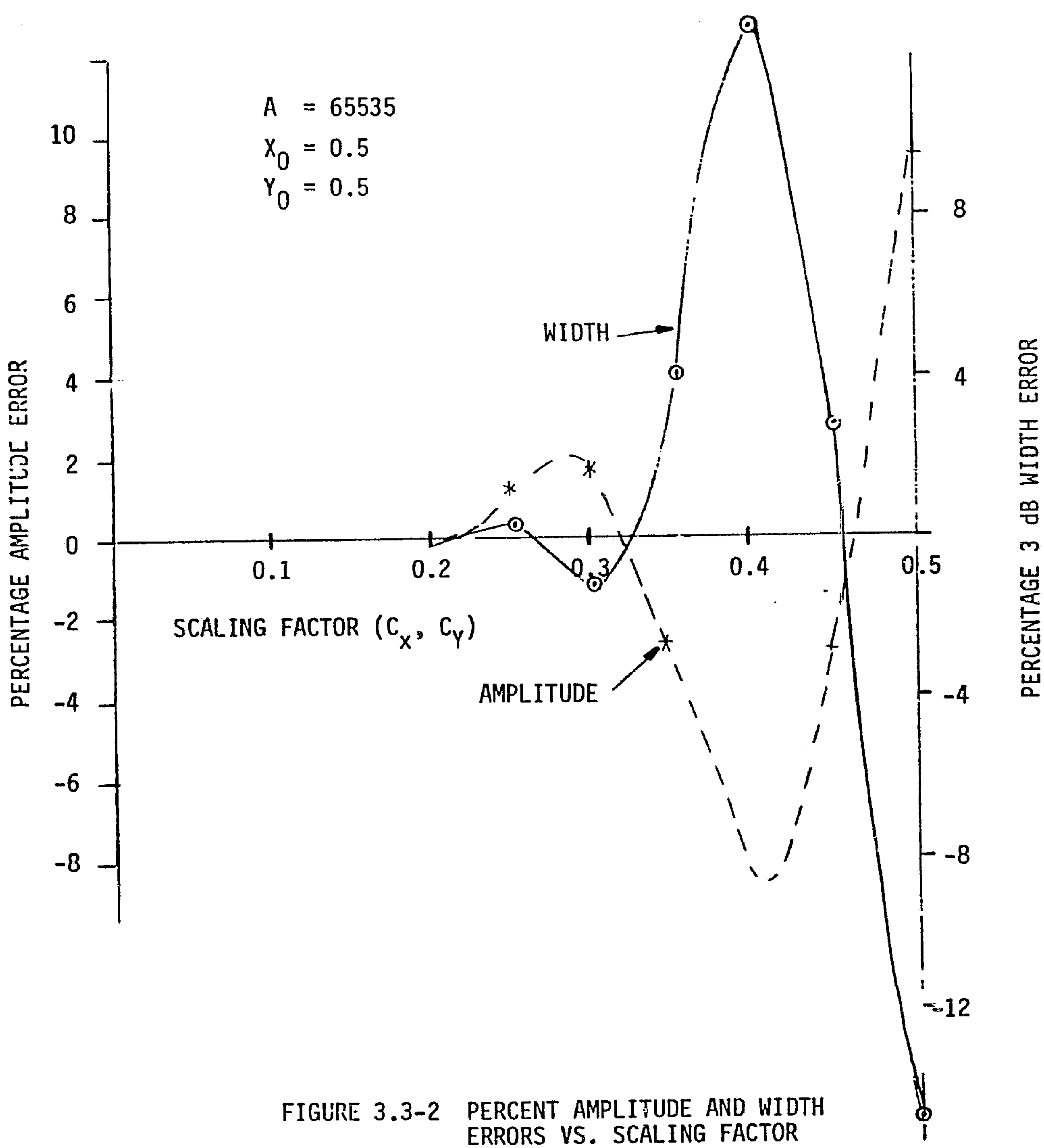

FIGURE 3.3-2 PERCENT AMPLITUDE AND WIDTH ERRORS VS. SCALING FACTOR

ORIGINAL PAGE IS
OF POOR QUALITY

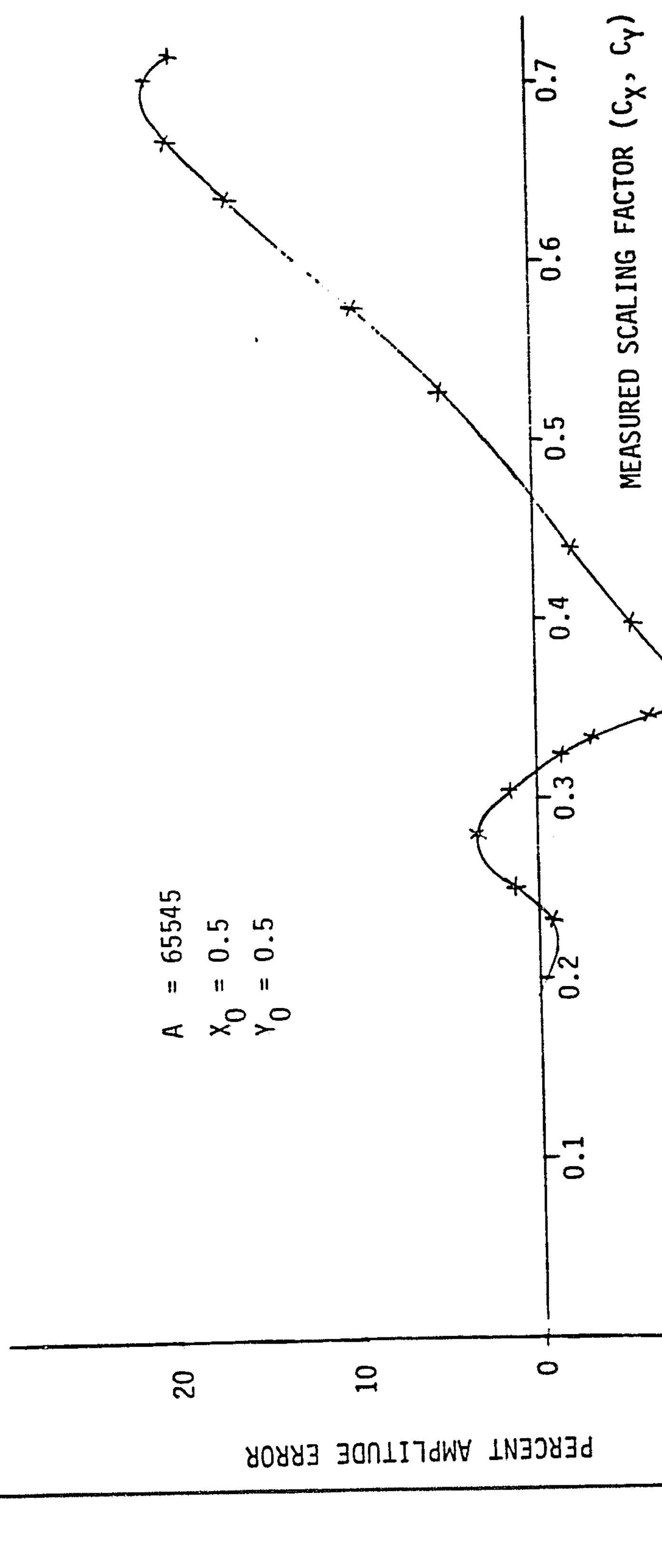

FIGURE 3.3-3 PERCENT AMPLITUDE ERROR VS. MEASURED SCALING FACTOR

The resulting measurements of amplitude and width were then compared with the known values and the errors recorded. Figure 3.3-1 shows how the amplitude measurement error varies as a funtion of the peak location within a pixel. The two curves represent the extremes of the errors; one is along a diagonal while the other is along the axis. The region between the two curves defines the range of possible errors. Figure 3.3-2 shows the percent amplitude error and percent 3 dB width error as a function of scaling factor for a peak location in the centre of the pixel (maximum errors). The errors are believed to be largely the result of aliasing due to the larger scaling factors; i.e, lower sampling rates. Combining the width measurement error and the true scaling factors allows the plot of percent amplitude error as a function of the measured rather than true scaling factors, and this is shown in Figure 3.3-3.

The procedure used for removing these systematic measurement errors was as follows:

- for a measured 3 dB width, convert to scaling factor and obtain amplitude error from Figure 3.3-3;

- depending on the measured peak location, scale the amplitude error by an amount obtained from Figure 3.3-1.

The resulting error estimate is converted to an amplitude correction factor, averaged for both the x and y dimensions, and this result it used to correct the measured amplitude.

As will be seen in the following section, the correction factors used were relatively small, this being the result of all but two of the measured targets having c_x and c_y values between 0.41 and 0.56. The largest correction factor was 0.6 dB, but most were approximately 0.1 dB.

3.4 Test Samples and Results

Two orbits were used for this evaluation:

- Orbit 416, July, 1978; and
- Orbit 882, August 27, 1978.

Orbit 416 was a descending pass, while 882 was ascending. The processed images (4 look amplitude summation) are shown in Figures 3.4-1 and 3.4-2. The scenes were processed under identical gain conditions.

Given the extremely large response of the receiving dish at the station, a test was performed on the SAR signal data to check the extent of data saturations in the analogue to digital converter (ADC). The test consisted of measuring the mean, standard deviation and percentage saturation of the IF signal data for Orbit 882 on digital CCT. The signal data is contained on a sequence of CCTs consisting of a total of 24,576 range lines of 13,680 samples starting at time 15:54:00,000 (GMT).

The signal response for the receiving dish was estimated to be located in the area bounded by lines 4352 to 8448 and samples 2750 to 4286, which is approximately the extent of the azimuth beam and range chirp. Measurements of mean, standard deviation, and percentage saturations were made on areas of size 256 lines by 512 samples throughout the estimated area. Table 3.4-1 gives the measured results. The percentage of samples saturated vary from a background level of 1 or 3% to 15 or 17% in the vicinity of the dish.

Figures 3.4-3 and 3.4-4 depict the percentage saturations as a function of range and azimuth respectively, through the region containing the receiving dish, the estimated position of which is marked. The SAR antenna beam pattern is readily apparent.

ORIGINAL PAGE
BLACK AND WHITE PHOTOGRAPH

FIGURE 3.4-1 GOLDSTONE IMAGE - ORBIT 416

ORIGINAL PAGE
BLACK AND WHITE PHOTOGRAPH

FIGURE 3.4-2 GOLDSTONE IMAGE - ORBIT 882

TABLE 3.4-1 SIGNAL DATA STATISTICS - ORBIT 882

First Line Number	First Sample Number	Mean	Standard Deviation	Percent Saturations
6145	1727	0.23	7.26	3.13
6145	2239	0.21	7.71	4.40
6145	2751	0.16	10.01	15.54
6145	3263	0.16	9.95	15.23
6145	3775	0.14	10.02	16.63
6145	4287	0.22	7.56	3.85
6145	4799	0.23	6.37	1.53
4097	3775	0.22	8.14	5.90
5121	3775	0.17	9.32	11.89
7169	3775	0.16	9.73	14.14
8193	3775	0.20	8.61	7.62
9217	3775	0.21	7.76	4.25

Each of the targets for both orbits were analyzed with graphs of impulse responses produced and measurements of target amplitudes made. Figures 3.4-5 to 3.4-12 show typical range and azimuth impulse responses for four of the reflectors.

Table 3.4-2 lists the amplitude results for each class of reflector. The figures for the 8'□ reflectors on orbit 416 are not applicable as they were not oriented appropriately. The error stated for the 8' Δ mean amplitude is the standard deviation of the samples, whereas the errors for the 6' Δ and 8'□ are maximum errors.

The amplitudes were then corrected for known systematic measurement error in the analysis software. Table 3.4-3 lists the measured amplitude, analysis error correction factor, and the corrected amplitude for each of the targets. The size of the correction factor varies from 0.93 to 1.02 (or -0.630 to 0.172 dB).

The corrected amplitudes are again listed for each target type in Table 3.4-4. Comparison to Table 3.4-2 shows some but not a general reduction in error deviations.

The most unreliable amplitude is that for the small 4' Δ reflector, as it is comparable in size to the background clutter in the cell. To remove this influence, an estimate of the clutter amplitude in the cell was made by measuring the response in a large desert area next to the target area. The mean power was measured as 120,925 with a standard deviation of 64,070. Subtracting this power estimate from the measured target lowers the target amplitudes from 1150 to 1100 and 800 to 720 for orbits 416 and 882 respectively.

It is also noted that the difference between the two orbits, as measured with the mean amplitudes for the 8' Δ reflectors, amounts to 1.10 dB. This may have resulted from a multitude of factors, including:

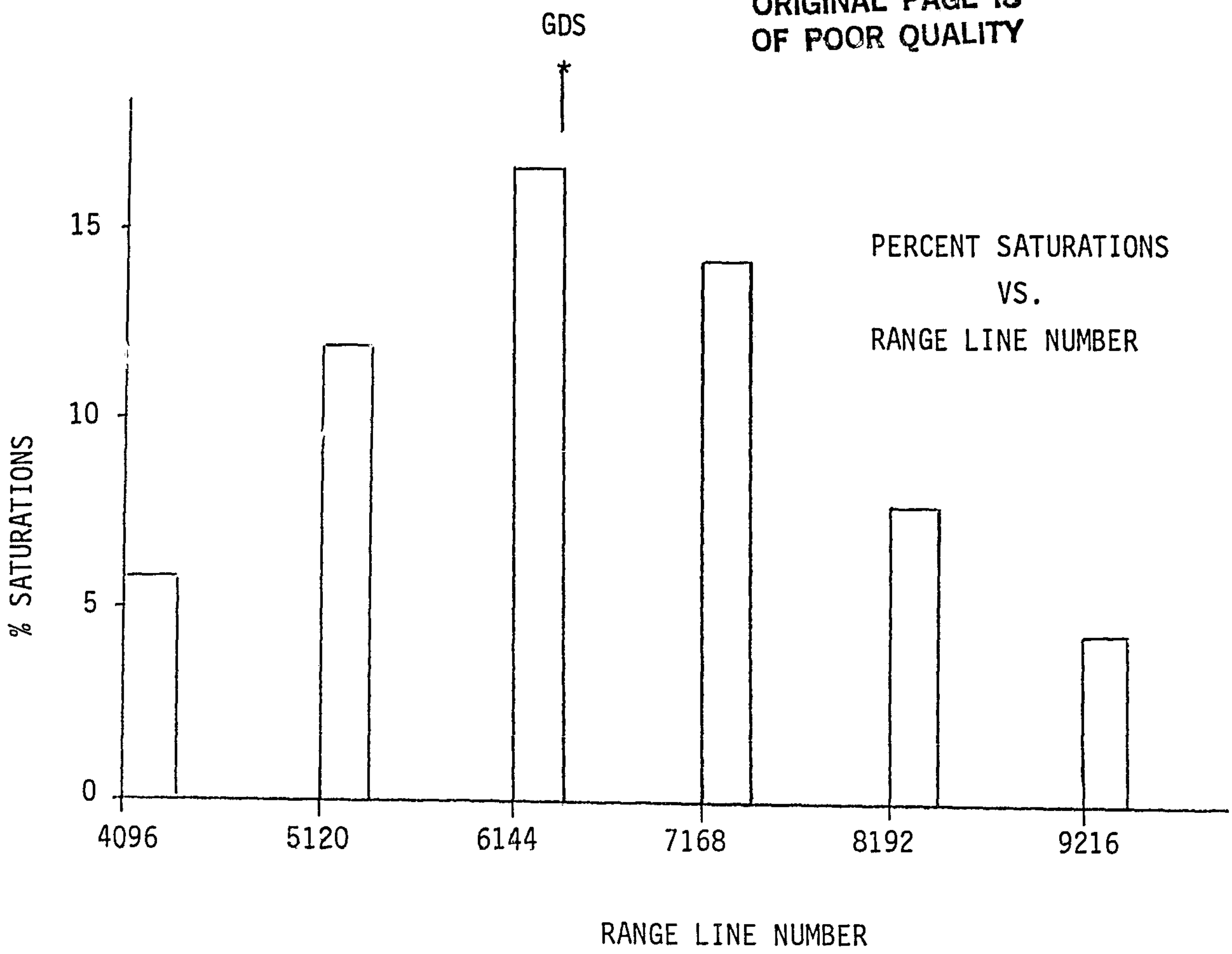

FIGURE 3.4-4 PERCENT SATURATIONS VS. RANGE LINE NUMBER

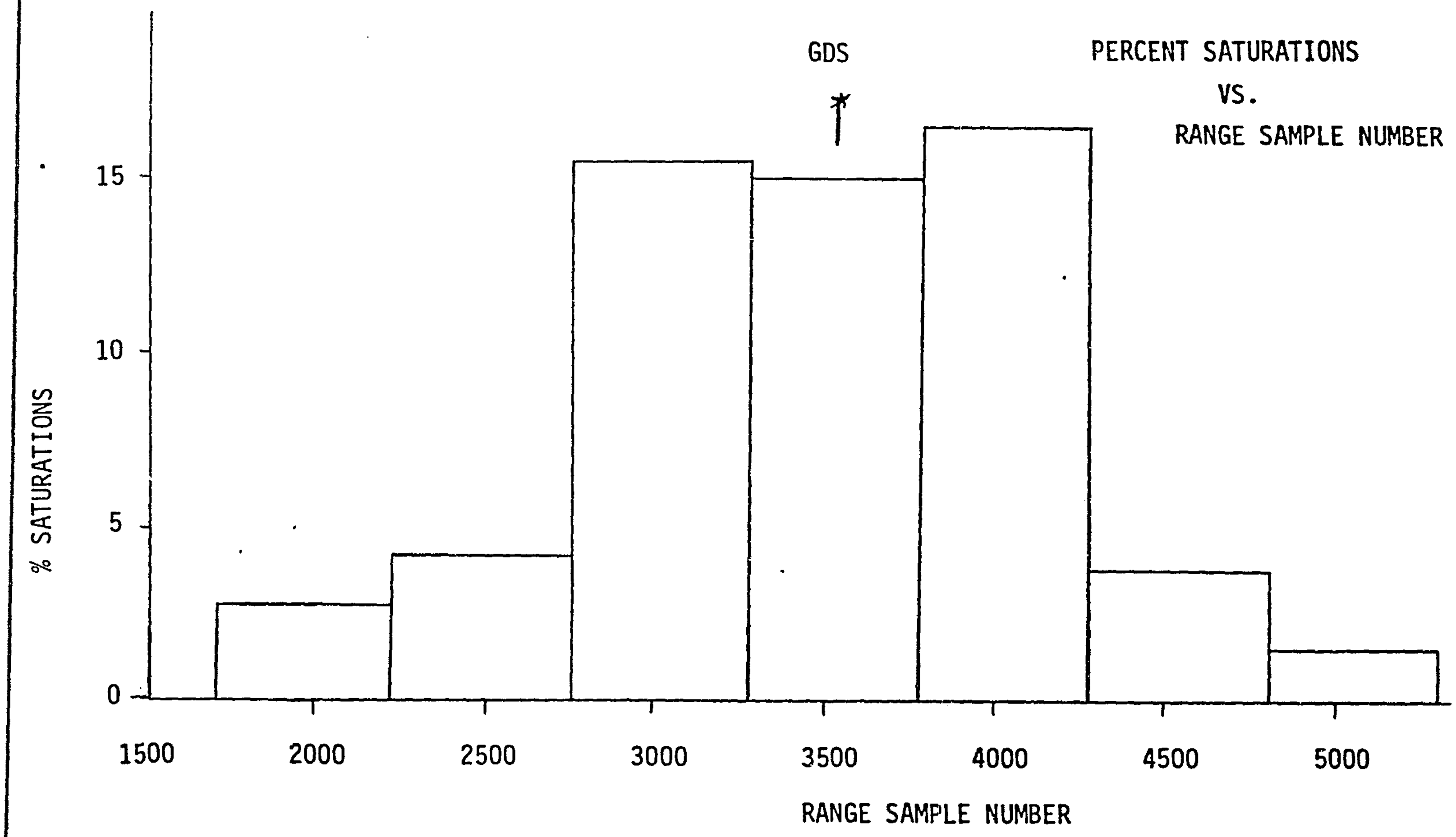

FIGURE 3.4-3 PERCENT SATURATIONS VS. RANGE SAMPLE NUMBER

ORIGINAL PAGE IS
OF POOR QUALITY

ORIGINAL PAGE IS
OF POOR QUALITY

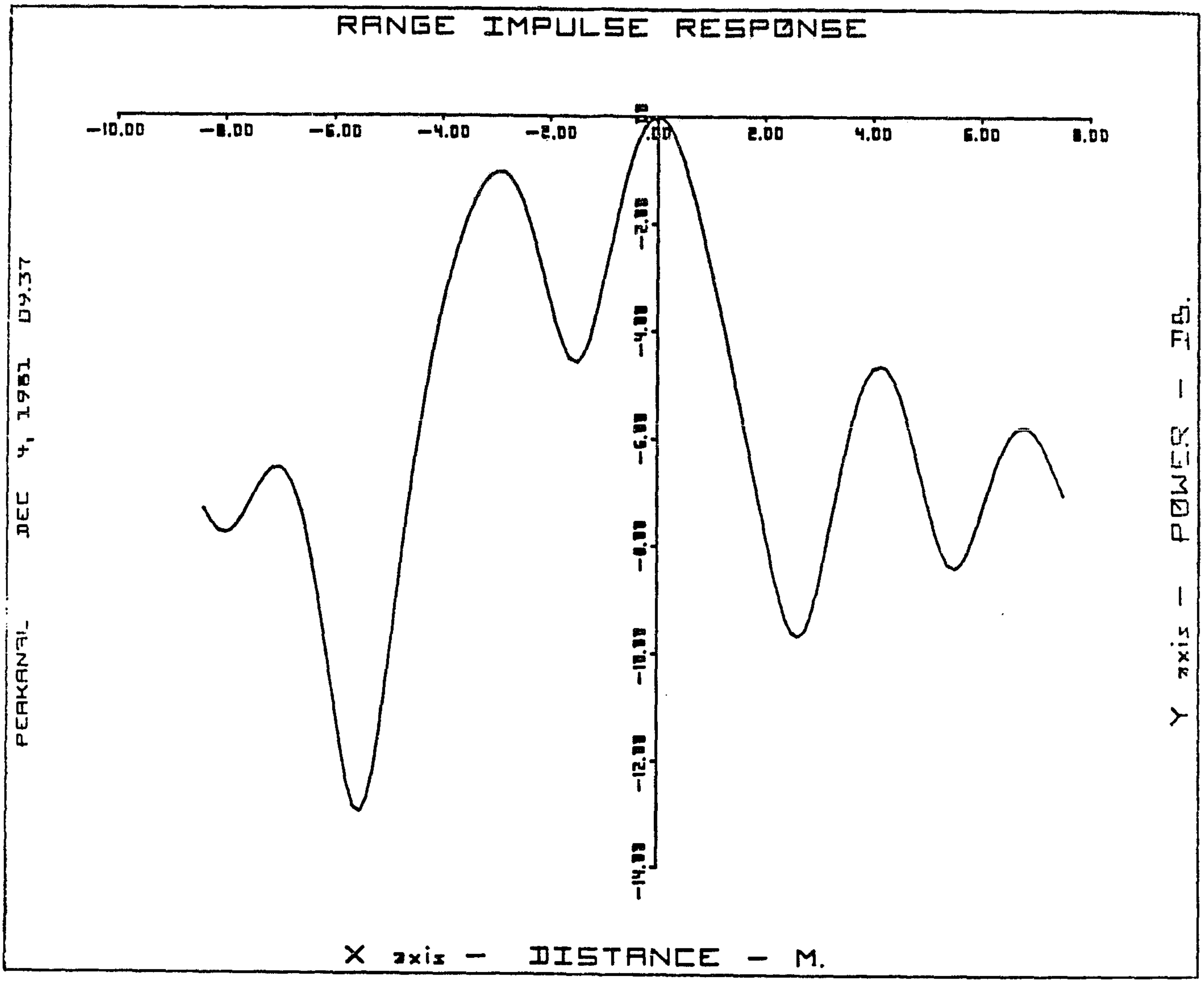

FIGURE 3.4-5 RANGE IMPULSE RESPONSE - TARGET A, ORBIT 882

ORIGINAL PAGE IS
OF POOR QUALITY

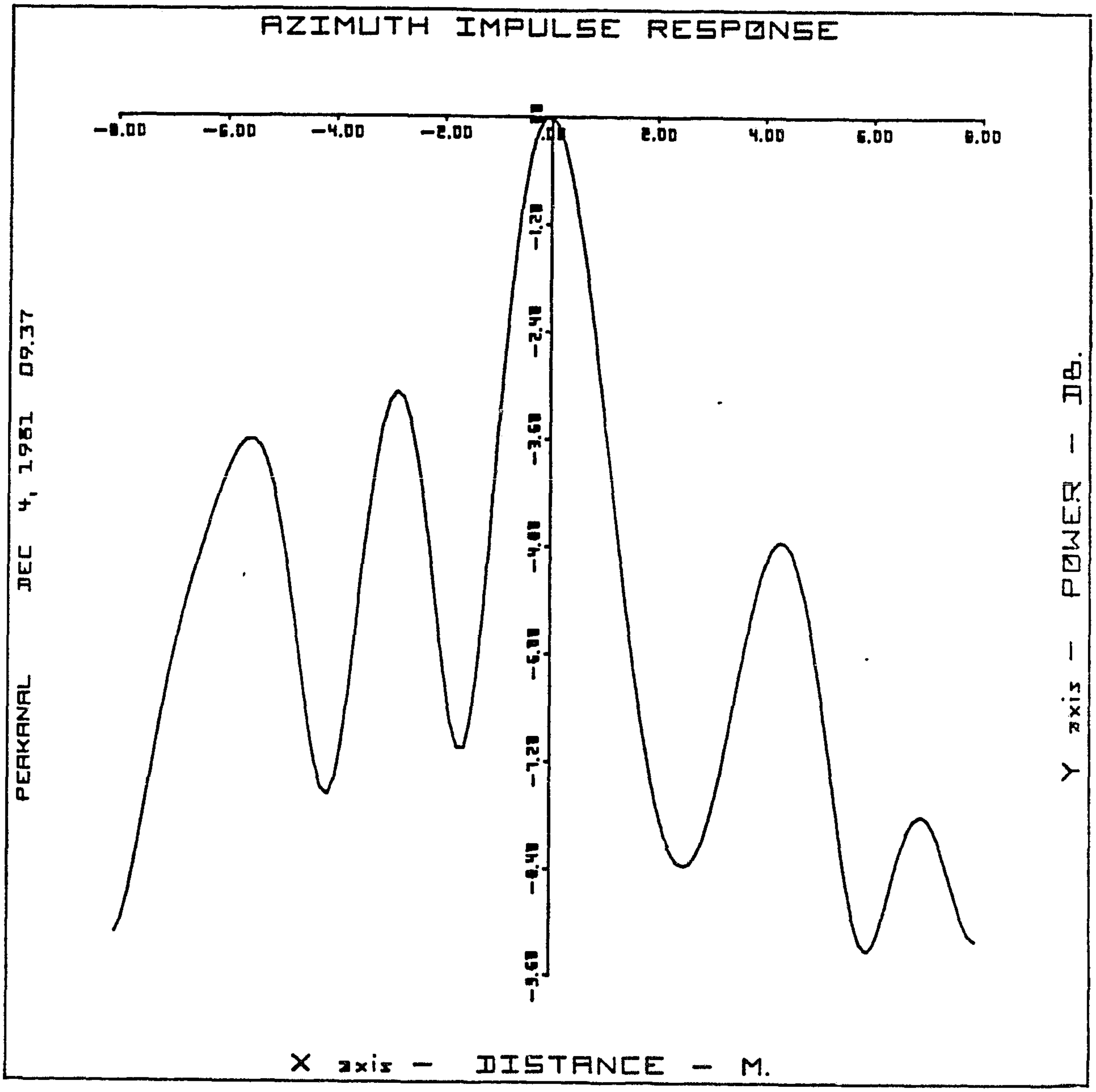

FIGURE 3.4-6 AZIMUTH IMPULSE RESPONSE - TARGET A, ORBIT 882

ORIGINAL PAGE IS
OF POOR QUALITY

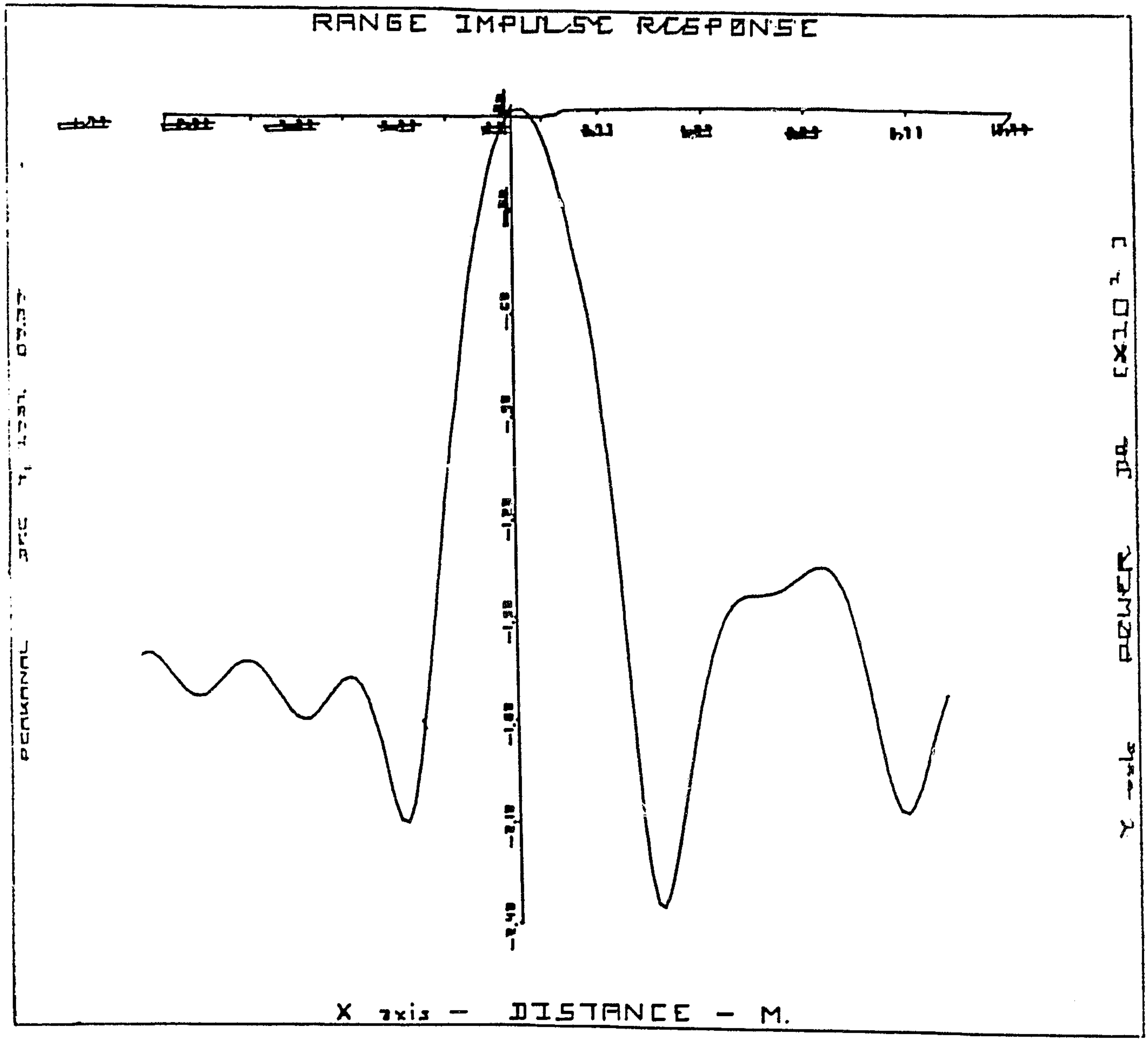

FIGURE 3.4-7 RANGE IMPULSE RESPONSE - TARGET D, ORBIT 882

ORIGINAL PAGE IS
OF POOR QUALITY

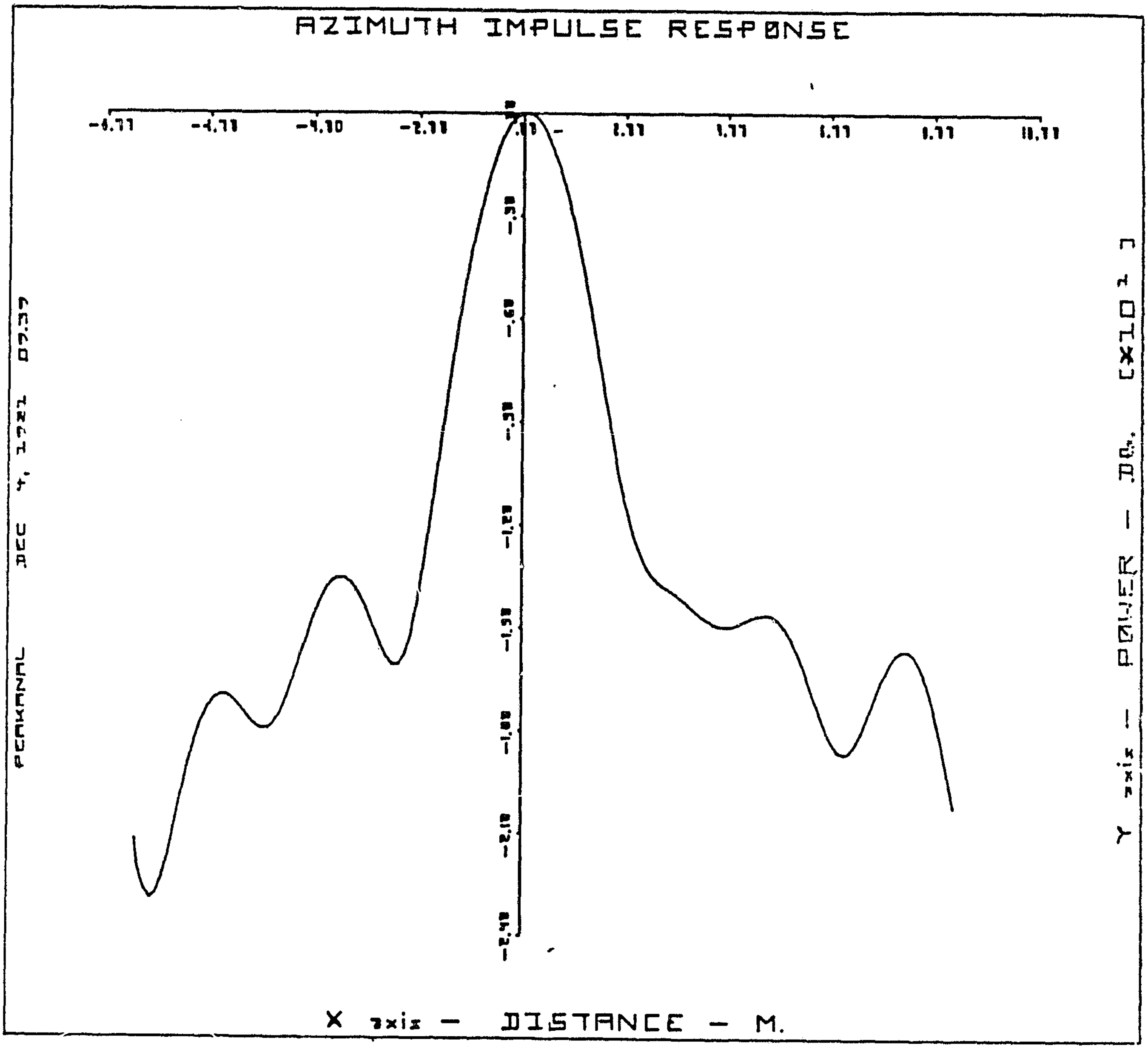

FIGURE 3.4-8 AZIMUTH IMPULSE RESPONSE - TARGET D, ORBIT 882

ORIGINAL PAGE IS
OF POOR QUALITY

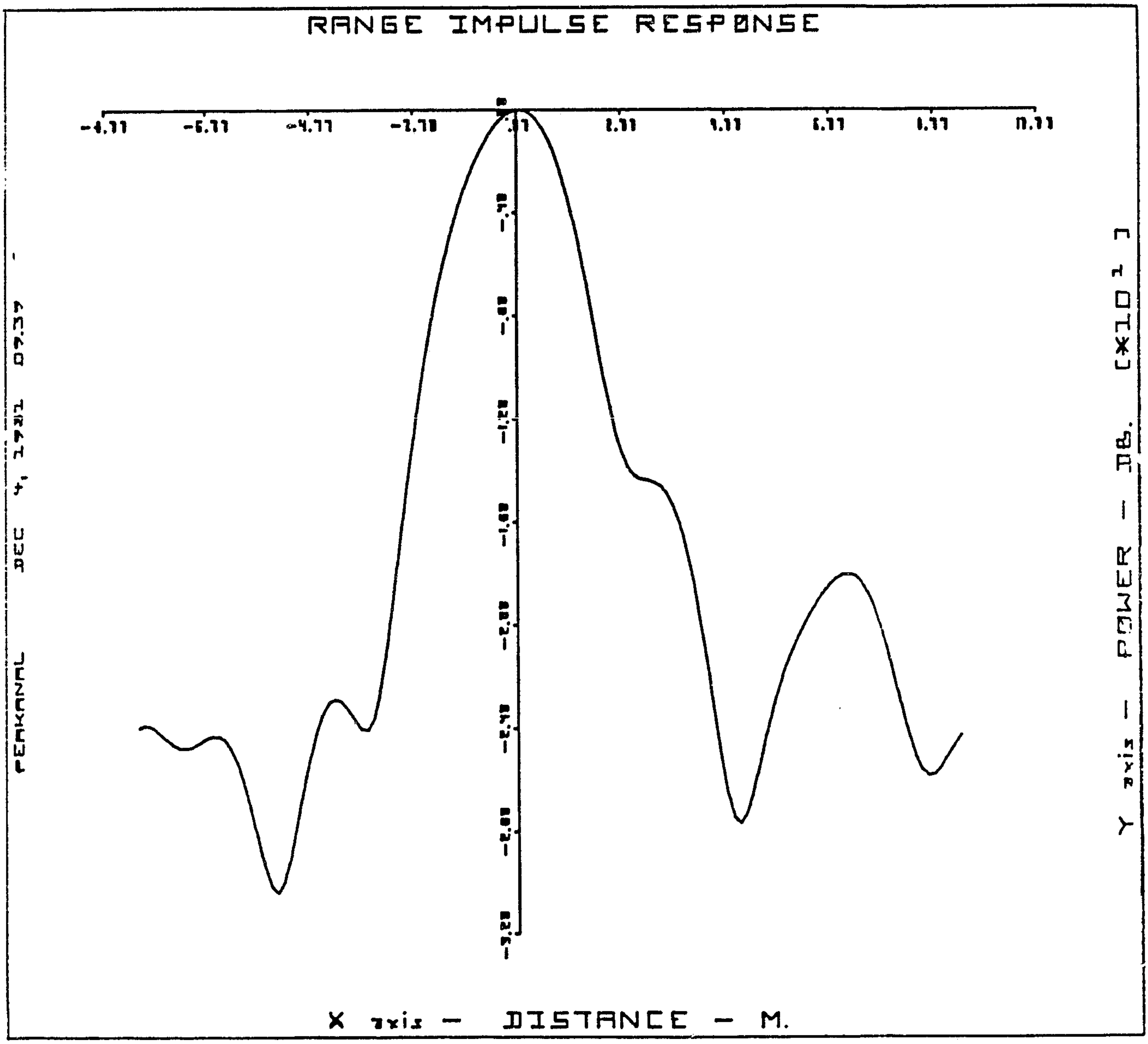

FIGURE 3.4-9 RANGE IMPULSE RESPONSE - TARGET E, ORBIT 882

ORIGINAL PAGE IS
OF POOR QUALITY

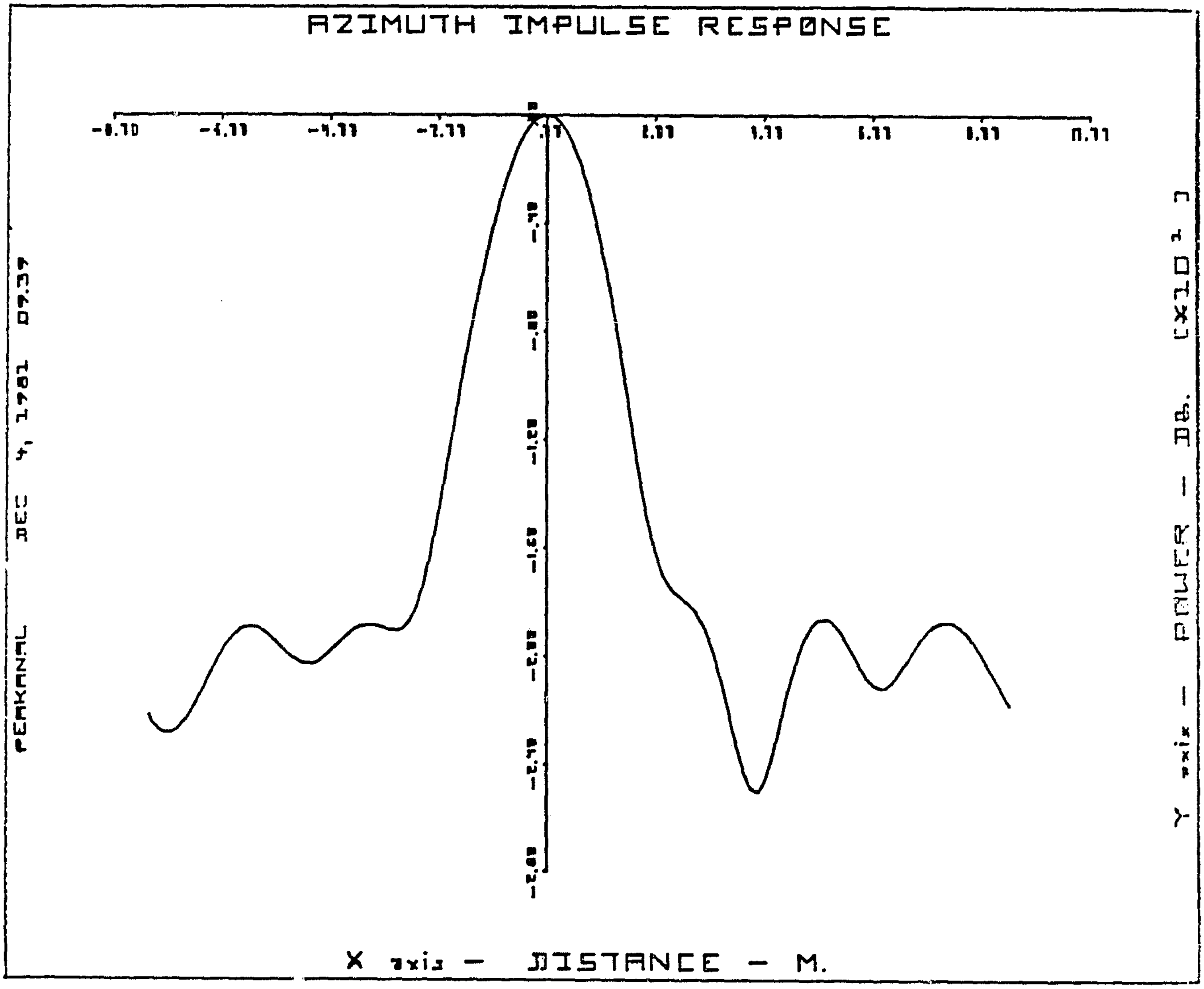

FIGURE 3.4-10 AZIMUTH IMPULSE RESPONSE - TARGET E, ORBIT 882

ORIGINAL PAGE IS
OF POOR QUALITY

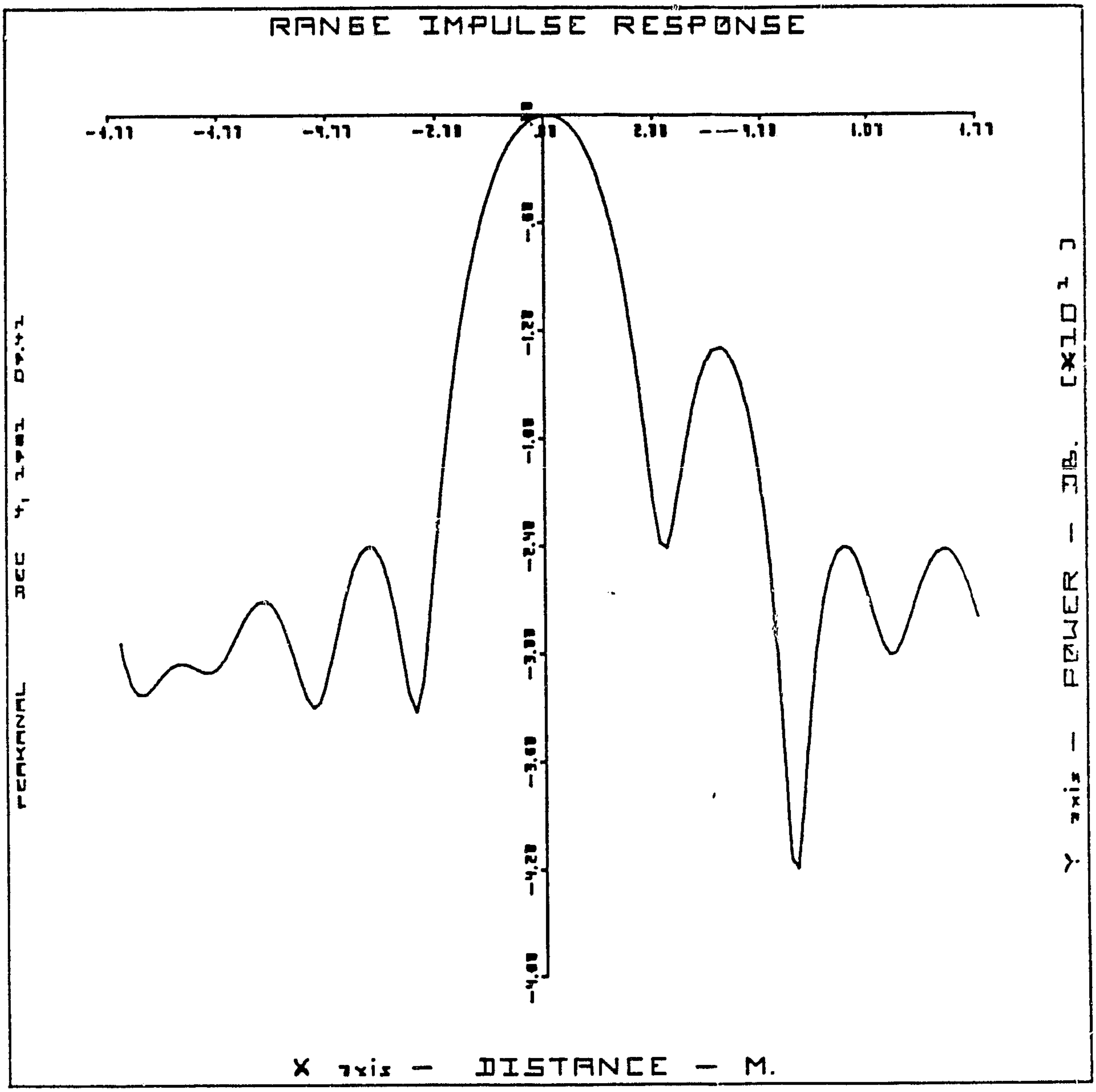

FIGURE 3.4-11 RANGE IMPULSE RESPONSE TARGET G, ORBIT 882

ORIGINAL PAGE IS
OF POOR QUALITY

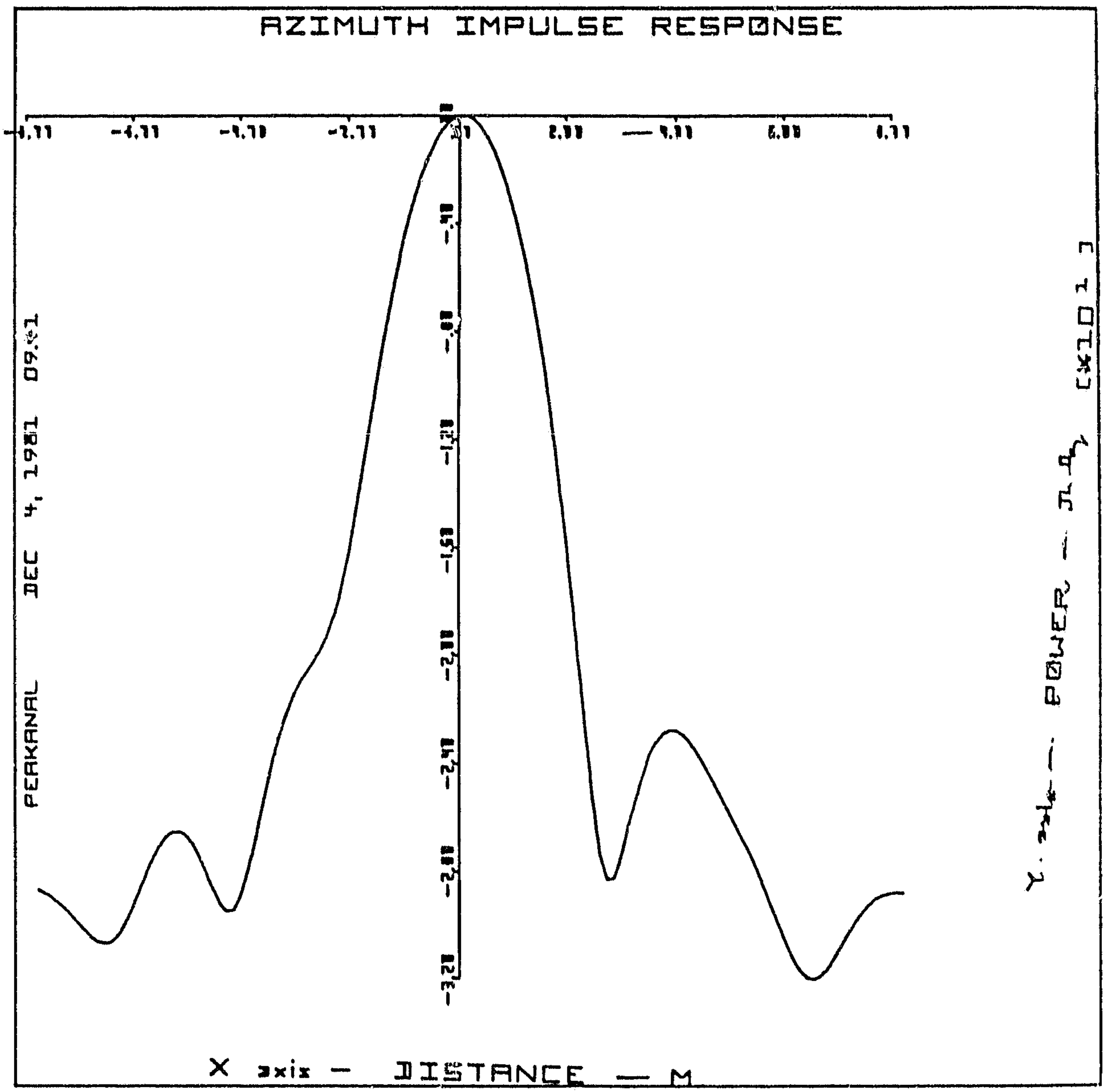

FIGURE 3.4-12 AZIMUTH IMPULSE RESPONSE - TARGET G, ORBIT 882

ORIGINAL PAGE IS
OF POOR QUALITY

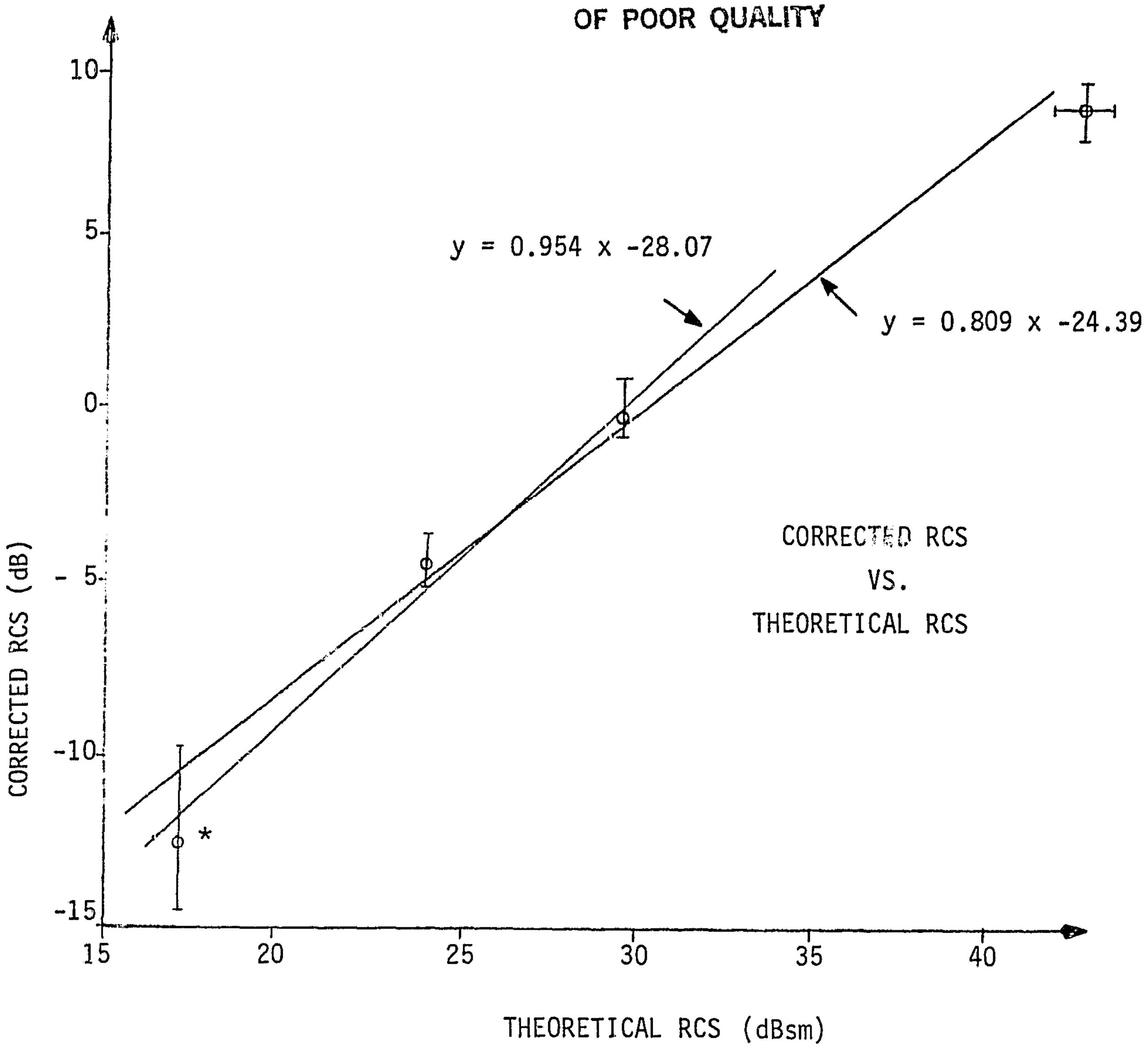

* ADJUSTED FOR BACKROUND CLUTTER

FIGURE 3.4-13 CORRECTED VS. THEORETICAL RCS

TABLE 3.4-2 MEASURED TARGET AMPLITUDES (ARBITRARY UNITS)

Orbit Number	Target Letter	Measured Amplitudes 4' Δ	6' Δ	8' Δ	8'□
416	A	1131.4			
	B		1893.5		
	C			3585.9	
	D		1973.0		
	E			3209.4	
	F			3312.7	
	G				—
	H			3448.1	
	I			3789.4	
	J				—
	Mean	1131.4	1933.3±39.7	3469.1±228.4	
882	A	782.5			
	B		2509.5		
	C			3870.0	
	D		2213.3		
	E			3606.1	
	F			3924.8	
	G				9576.6
	H			4112.6	
	I			3881.6	
	J				11933.1
	Mean	782.5	2361.4±148.1	3879.0±181.1	10754.8±1178.3

TABLE 3.4-3 AMPLITUDE CORRECTION

Orbit No.	Target Letter	Measured Amplitude (Arbitrary Units)	Analysis Error Correction Factor	Corrected Amplitudes (Arbitrary Units x 103)
416	A	1131	1.02	1.15
	B	1894	1.01	1.91
	C	3586	0.99	3.55
	D	1973	0.98	1.93
	E	3209	1.00	3.21
	F	3313	0.97	3.21
	G	—	—	—
	H	3448	1.00	3.45
	I	3789	0.93	3.52
	J	—	—	—
882	A	782	1.02	0.80
	B	2510	1.01	2.54
	C	3870	0.99	3.83
	D	2213	1.00	2.21
	E	3606	1.00	3.61
	F	3925	1.00	3.93
	G	9577	1.00	9.58
	H	4113	0.98	4.03
	I	3882	0.99	3.84
	J	11933	1.01	12.0

TABLE 3.4-4 CORRECTED AMPLITUDES

Orbit Number	Target Letter	4' Δ	Corrected 6' Δ	Amplitudes 8' Δ	8'□
416	A	1150			
	B		1910		
	C			3550	
	D		1930		
	E			3210	
	F			3210	
	G				—
	H			3450	
	I			3520	
	J				—
	Mean	1150	1920±10	3390±166	—
882	A	800			
	B		2540		
	C			3830	
	D		2210		
	E			3610	
	F			3930	
	G				9580
	H			4030	
	I			3840	
	J				12000
	Mean	800	2375±165	3850±156	10790 ±1210

- differences in sensitivity time control setting;
- differences in automatic gain control;
- temperature/gain fluctuations between passes; and
- spacecraft roll causing slight antenna gain difference.

Upon adjusting the 4' Δ reflector amplitude for clutter and normalizing the results to the mean value of the 8' Δ reflectors for the appropriate orbit and expressing them in dBs, Table 3.4-5 is obtained. These results are plotted as a function of the theoretical RCS in Figure 3.4-5. The vertical bars show the range of values. Linear regressions were performed on the results. As the large 8'□ reflectors were not designed for calibration purposes, but rather as "finders" for the array, two regressions were done; i.e., with and without the 8'□ results. The results for the form $y = Ax + B$ were as follows:

With 8'□	$y = 0.809\ x - 24.39$	$r = 0.972$
Without 8'□	$y = 0.954\ x - 28.07$	$r = 0.970$

where:

y = corrected RCS (dB - arbitrary units)
x = theoretical RCS (dBsm)
r = correlation coefficient ($-1 \leqq r \leqq 1$)

TABLE 3.4-5 CORRECTED RCS

Orbit Number	Corrected RCS 4' Δ	6' Δ	8' Δ	8'□
416	- 9.77*	-4.97	0.40	
		-4.87	-0.47	
			-0.46	
			0.15	
			0.97	
882	-14.6 *	-3.62	-0.04	7.92
		-4.80	-0.56	9.92
			0.17	
			0.41	
			-0.01	
Theory	17.17	24.09	29.63	42.8!1

* Adjusted for background clutter.

3.5 Summary and Conclusions

An amplitude calibration was performed with imagery of the Goldstone target array, as processed by the MDA Seasat SAR processor (AP version). The data from two orbits (416 and 882) were utilized.

Examination of the IF signal data showed significant saturations on the order of 16 percent in the vicinity of the Goldstone receiving dish, as compared to a backround level of 2 or 3 percent. It is possible but considered unlikely that this has caused some non-linearities to be induced in the target array amplitudes. It should be noted that this by no means precludes the possibility that non-linearities were induced prior to the ADC.

The measured amplitudes were corrected for systematic errors in the analysis software, as well as for backround clutter. A linear regression of the corrected RCS against the theoretical RCS resulted in a slope of 0.954 with a correlation coefficient of 0.970. Single pass linearity was good despite considerable saturation in the signal data. There was also fairly good pass-to-pass stability with a 1.10 dB gain variation.

4. NEW TECHNOLOGY

There were no reportable new technology items under this contract.

5. REFERENCES

[1] Richardus, P. and R. K. Adler. Map Projections for Geodesists, Cartographers and Geographers. North Holland, 1972.

[2] Seasat-A SAR Design Verification Report, August 15, 1977. JPL, 622-31.

[3] Private communication with Mr. Ed Caro, JPL.

[4] Seasat-A Instrument Data Processing System Detail Functional Specification, Vol. 2, PD 622-14, JPL, May 1977.